Spring 5-18-2018

A Numerical Study in Prediction of Pressure on High-Speed Planing Craft during Slamming Events

Shivank Srivastava
University of New Orleans, ssrivast@uno.edu

A Numerical Study in Prediction of Pressure on High-Speed Planing Craft during Slamming Events

A Thesis

Submitted to the Graduate Faculty of the
University of New Orleans
in partial fulfillment of the
requirements for the degree of

Master of Science
in
Engineering
Naval Architecture and Marine Engineering

by

Shivank Srivastava

B.S. Birla Institute Of Technology and Sciences, Pilani,2014

May, 2018

Acknowledgments

First of all, I would like to acknowledge Dr William S. Vorus whose theory forms the premise of this work and a sincere acknowledgment to all the scientist who have been contributing in this particular topic, I wish to offer my small invaluable contribution.

The Louisiana State Board of Regents (Industrial Ties Research Subprogram [LEQSF(2015-18)-RD-B-09]) should be thanked for sponsoring this research. Also, this project would not be possible without the skill and generosity of Metal Shark Boats in providing the model for tank testing.

I would like to express my deepest gratitude to my advisor Dr. Brandon M. Taravella, for believing in me and providing me with an opportunity to work for him and carry out this research. His teachings have always been an encouragement for me in overcoming roadblocks that have come up during the course of this research. He has always been a strong pillar of support through tough times. His technical and editorial advice was essential in completion of this thesis and has taught me innumerable lessons on workings of academic research. I wish to continue collaborating with him for my future works.

Dr. Lothar Birk and Dr. Kazim Akyuzlu, also deserve thanks for agreeing to participate in my thesis committee. Dr. Birk's valuable advice on 'Fortran' programming has been important factor in completing this thesis. A special thanks to Dr. Akyuzlu for providing me with an opportunity to do future research under him. It will be an educational experience.

The UNO School of NAME staff members Ryan Thiel and George Morrissey who have helped me throughout my research, I am grateful for their help. My dear friends and colleagues Jonathan Eastridge and David Bonneval with whom I have collaborated to work on this project. They have been there in tough and good times and have helped me beyond the scope of their obligations. Their suggestions and comments have been very valuable in this thesis.

I would also like to thank Ms. Manika Bhondeley for helping me both professionally and personally by offering invaluable inputs and strength day and night throughout the journey of this thesis. Her work ethic has always been a source of motivation.

Last but not the least I would like to thank my family for their constant support and strength that they have provided during tough times which has made me ovecome the obstacles.

Table of Contents

List of Figures

List of Tables

Abstract

This thesis is an attempt to create a computer based tool that can be used academically and later industrially by naval architects in analysis and development of efficient planing hull forms. The work contained here is based on the theory created by Vorus (1996) which falls between empirical asymptotic solutions and intractable non-linear boundary value problem in the time-domain. The computer code developed predicts pressures on the bottom of high-speed planing craft during slamming events. The code is validated with available numerical data as a benchmark case. An aluminum wedge is dropped from various heights resulting in unsteady pressure distributions with high peak over the bottom plate. These pressure distributions are compared to the numerically predicted pressures by the code and presented in this thesis. The predicted flow velocities are within 8% difference of experimental data. The graphs depicts similar trends in experimental and numerical data. The predicted peak pressures deviate within 4% to 20% from experimental data. The analysis and comparison illustrate efficacy of the code.

Keywords: Slamming, code, high-speed, planing, non-linear, pressure, asymptotic, boundary value, experimental, numerical

Chapter 1

Introduction

It is due to the nature of waves that the bow of a marine craft rises above the water and subsequently enters back into water. While re-entering, the contact region between the fluid and body surface expands quickly. This event is accelerated for high-speed craft. The sudden acceleration of fluid close to the hull surface is responsible for developing high pressures and forces. This event is called '*slamming*'. The hydrodynamic forces developed due to slamming are high enough to influences the physics of fluid flow around the hull and cause temporal deflection of bottom shell plating. The magnitude of these forces can cause irreparable deflection or damages if the structural design is flawed or slamming effects are not properly considered during the design phase.

The study of flow physics during slamming has been of interest for many years. While in the initial stages of hull design, the essential parameters, like lift to drag ratio, power, speed, resistance, etc. are needed which can be readily determined if the hydrodynamic forces acting on basic shapes are known. The studies conducted date back to Von Karman (1929), who used the concept of *added mass* to determine these forces. His work formed the basis for the studies conducted until today.

Predicting the pressure distribution caused during slamming events is known to be an efficient way of determining the forces. It also helps in resolving the structural arrangement of planing vessels so that they are light enough to skim without loosing their structural integrity. These predictive pressures play a significant role in determining the essential parameters for the design. Hence naval architects require an economical, efficient, easy and user friendly tool to analyze planing surfaces with variable geometric hull forms that have

not been covered in past semi-empirical research.

Analytical methods proposed by Wagner (1932) provide exact solutions for simplified impact problems but the necessary calculations are very tedious. However, these methods necessitate geometrical similarity and easily predict infinite pressure or infinite pressure gradients at geometrical discontinuities. Computational Fluid Dynamics (CFD) methods do not encounter such problems. CFD codes or commercial packages use more approximation methods to provide more agreeable results to analytical solutions, such as Reynolds Averaged Navier Stoke (RANS) equation solvers. However, special training is required to operate these packages. The computation time to solve impact problems using CFD software is great and expensive. The computational power requirements are also not available to all at a low cost. On the other hand, writing one's own CFD code requires knowledge, not only from realm of naval architecture, but also from various branches of engineering and computer science. Hence the purpose of this study is to: (1) develop a computer code which is user friendly and predicts the pressures on high-speed planing vessels during slamming events, (2) analyze the flow physics caused by impact and (3) to improve the hull form of planing crafts. This thesis also forms a basis for further development of the code to incorporate steady planing as attempted by Savander et al. (2002) and to be developed into a commercial package to be easily used by naval architects to analyze and design planing crafts hull forms more efficiently.

The study conducted here includes numerical hydrodynamics coupled with experimentation to validate the results. This thesis is an attempt to understand and create a computer code based on Dr. William S. Vorus' theory (Vorus 1996), as a tool which can be used academically and further developed on an industrial basis. For a successful completion of the this thesis, the non-linear boundary value problem equations developed by Vorus are discretized into an algebraic set of equations, and a computer program coded in the programming language 'Fortran' is utilized to solve them. To validate the code, solution parameters were compared with Vorus' data and further authenticated with experimental data. The experi-

ments performed are mentioned as wedge drop experiments in (Eastridge 2017) which is a branch of the same ongoing research at the University of New Orleans.

1.1 Literature Survey

Prediction of flow physics of water during impact of cylindrical vessels with approximately flat bottom has been of interest since the 19^{th} century. The studies date back to early 1900 by Karman (1929) during the development of sea planes or flying boats. He developed an asymptotic solution for the purpose of studying the structural behavior caused by stresses during impact landing of sea planes. Von Karman assumed zero gravity, ideal flow formulations, and that hydrodynamic perturbations are small as compared to the hull cross section. This led to a simplification of the full three dimensional boundary value problem into a problem solved in two dimensions.

Wagner (1932) modified Karman (1929) asymptotic solutions to analyze the pressure distributions. He expanded the model by taking into account the pressure due to water build up between the undisturbed free surface and wedge contour know as the *jet rise* or *spray-root* development. Wagner also introduced the concept of the so-called wetting factor which is also used in this thesis and will be discussed later. The spray root is responsible for a spike in hydrodynamic pressure. His model was an infinitely long expanding wedge, with no chine and series expansion defining the contour geometry. Wagner avoided singularities in the pressure distribution by proposing an asymptotic technique which surpasses the appearance of singularities in the inner solution domain. The work of Wagner provides basic practical solution techniques to real problems and formed the basis of subsequent research until today.

Von Karman and Wagner asymptotic solutions are only valid when geometric similarity is present. Other researchers such as Cointe (1991) and Zhao and Faltinsen (1993) include the assumption of flow similarity with an asymptotic approach. Complexity arises with an increase in transverse flow perturbation with non-linearity as the flatness of the cylinder

increases. Zhao and Faltinsen (1993) were able to compute the non-linear boundary value problem with reasonable accuracy, but only for a special semi-infinite wedge cylinder.

Vorus (1996) developed a solution method which is a rational compromise between direct numerical inversions of the exact governing equations and the simple asymptotic theories which evolved from the work of Wagner. Vorus considered the large flow perturbations during impact making the model hydrodynamically non-linear and geometrically linear by satisfying the boundary conditions on the flat cylinder axis. He incorporated a non-linear term in the pressure prediction using numerical time integration. Vorus model is "a compromise between the computational intractable time-domain solution of the exact non-linear ideal flow boundary-value problem and the simple, but overly restrictive, asymptotic solutions" (Vorus 1996). His method is the closest to the solution required to deal with the problem practically as it does not require geometric similarity in two dimensions. His main contribution was developing equations which allow for variable deadrise angle along the cylinder.

Savander et al. (2002) redefined the theoretical and numerical formulation of Vorus for the perturbation potential, perturbation velocities and vortex sheet strength. The work presented by Savander was very close to Tulin (1957). Tulin correctly defined general three-dimensional flow problems to be modeled in two dimensions. He was able to predict drag and lift for a slender prismatic shape hull form. This formed the basis for Vorus' and Savander's research. Savender attempted to incorporate Vorus' theory and extended Tulin's work to predict lift and drag on a high-speed planing vessel. The model he developed not only allows variation of deadrise angle transversely but also longitudinally.

A lot of experimental studies are conducted to study the slamming events. These are commonly called wedge drop experiments. Judge et al. (2004) performed experiments on an aluminum wedge with length of 1.509 feet and width of 0.656 feet with a deadrise angle of 37^o. Cases for the initial asymmetric wedge impact flows were examined with both horizontal and vertical velocities. The boundary-value problem was modeled by method of two dimensional vortex distribution. Experimental drop tests provide an understanding of the initial

flow separation off the wedge vertex when horizontal-vertical impact velocities (asymmetric impact velocities) are present. The Numerical method was also designed and validated with experimental data for small degrees of asymmetry and small ratio of horizontal to vertical impact velocity.

Eastridge (2017) also conducted an experimental investigation to study the hydroelastic response of an aluminum wedge. The model in consideration is discussed in detail further in this thesis. Digital Image Correlation (DIC) technique was used to examine the deflection on the bottom shell. The DIC code was validated with data collected from strain gauges. During the model tests pressure data was recorded with pressure sensors and is used to compare the numerical result obtained with the code developed in this thesis. The experiments were performed in the towing tank of the University of New Orleans.

This further forms the scope of this thesis, to incorporate Tulin (1957), Vorus (1996) and Savander et al. (2002) in the computer code developed here. With the relation known between the time-domain impact flow and longitudinal flow this approach is possible. This code could be made available as a user friendly tool that can be used on an industrial basis by naval architects in designing forthcoming high-speed planing vessels and improving existing designs.

Chapter 2

Physics Explained

The hydrodynamic model formulated here is considered to be ideal incompressible flow without gravity. This has been common practice in past theoretical impact research (Vorus 1996). For convenience as per Figure 2.1 z axis is horizontal, lies on water surface and y axis is vertical. The downward motion is considered to be positive. The geometric model in consideration is a wedge whose continuous contour terminates at a hard knuckle chine Z_{ch}. Due to hard chine the impact flow is separated at Z_{ch} as in Figure 2.2. The velocity of wedge $V(t)$ is specified for the calculation and the height between undisturbed free surface and keel is $Y_{wl}(t)$.

As per Vorus (1996), on impact of a wedge cylinder, the free surface turns back under the contour forming an initially attached jet 'spray root' as in Figure 2.1. The spray root point B, with coordinate $Z_b(t)$, advances rapidly outwards with point C, with coordinate $Z_c(t)$ following behind. In the impact phase also known as 'Chine-Unwetted' or (CUW), the contour pressure distribution has a sharp spike and large negative pressure gradient into point C. This is because of the jet-rise. $Z_c(t)$ is also the point of zero contour dynamic pressure. On reaching the chine, also called 'Chine-Wetted' or (CW) flow as in Figure 2.2, point C comes to an abrupt halt, $Z_c(t) = Z_{ch}$, and stays same until the deceleration effects initiates the return of keel. *The theory described here is valid upto this moment* The chine-wetted phase is characterized initially by rapidly decreasing pressure gradient on the cylinder contour, then leveling towards temporally constant cylinder pressure distributions as the penetration progresses.

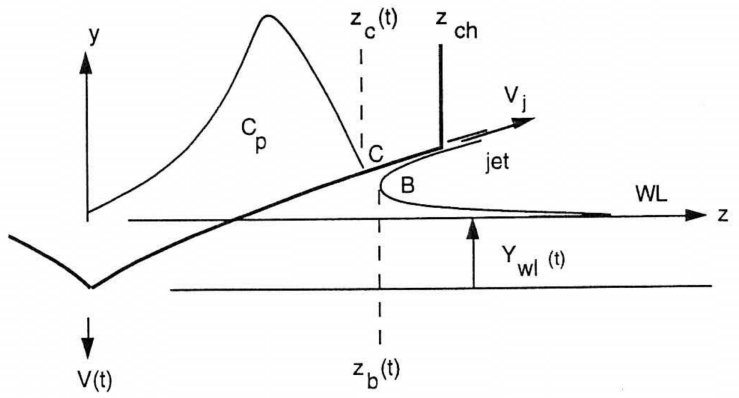

Figure 2.1: Cylinder impact, chine unwetted case (CUW) (Vorus 1996)

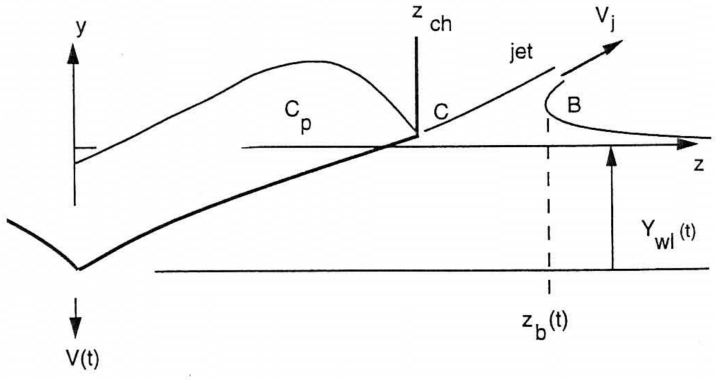

Figure 2.2: Cylinder impact, chine wetted case (CW) (Vorus 1996)

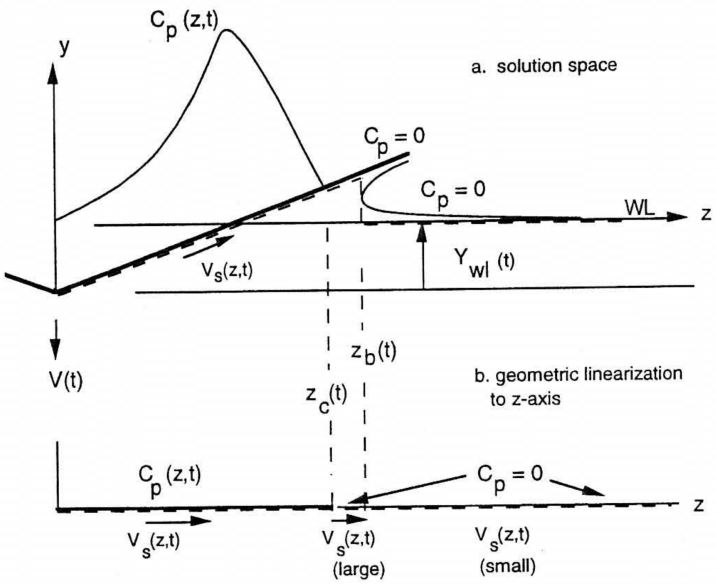

Figure 2.3: Physical Description (Vorus 1996)

2.1 Mathematical model

The velocity of the spray jet in Figure 2.3 is higher than the impact velocity and the velocity on the asymptote, which forms the upper branch of the free surface and extends to infinity in z axis, is lower than impact velocity. This difference in velocities is exploited as, the tangential velocity on approaching the z axis from below and outside of B is zero. This limiting physics forms the mathematical model (Vorus 1996) as shown in Figure 2.4. Hence the boundary conditions are as follows: (1) $C_p = 0$ beyond $Z_c(t)$, (2) *the jet fluid domain from B outwards is discarded* and (3) V_s beyond $Z_b(t)$ on the undisturbed surface is *very small.*

The cylinder flatness is exploited by collapsing it onto the z-axis so as to satisfy the boundary conditions. During chine-unwetted flow as per Figure 2.3 fluid exits with very large $V_s(z,t)$ near $z_c(t)$ and extends into the region $z_c \leq z \leq z_b$ where velocity drops to a lower order magnitude due to the abrupt halt in zero pressure point due to slope discontinuity at the hard chine where flow is forced to separate.

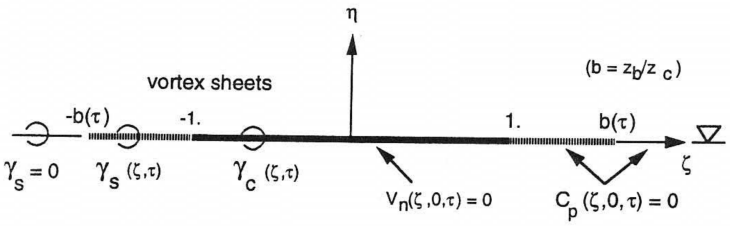

Figure 2.4: Mathematical Model (Vorus 1996)

2.1.1 Order Of Magnitude

As per Vorus (1996) the deadrise angle may vary throughout the cross section of the contour however, for simplicity in writing the code and performing the experiments, the deadrise angle of the contour is considered to be constant. Contour velocities V_n and V_s or alternatively represented as a function of perturbation velocities v & w. The normal and tangential velocities are defined in terms of perturbation and contour velocity as follows (Vorus 1996):

$$\begin{aligned} V_n &= (V+v)\cos\beta - w\sin\beta \\ V_s &= w\cos\beta + (V+v)\sin\beta \end{aligned} \tag{2.1}$$

On the basis of prevailing physics (Vorus 1996) defined that the transverse velocity, w, is an order of magnitude higher than the vertical velocity on the cylinder, but drops two orders to the free surface beyond the spray root hence going extremely small and of same order as v. On the cylinder contour V_n is 1^{st} order by equation(2.1), but forced to zero by the kinematic boundary conditions. The tangential and normal velocities can be summarized as:

$$\begin{aligned} V_n &= 0 && z_c \le z \le z_b, z_c < Z_{ch} \\ V_n &= V && z_c \le, z_c = Z_{ch} \\ V_n &= V, V_s = 0 && z_b \le z, z_c \le Z_{ch} \end{aligned} \tag{2.2}$$

2.1.2 Theoritical Formulation

Velocities are non-dimensionalized with the impact velocity V_0, and all linear dimension with thw chine offset Z_{ch}. The time is also non-dimensionalized as $\tau = V_0 t/Z_{ch}$. By Equation(2.2), zero tangential velocity ensures zero free-surface pressure. The remaining boundary condition is satisfied with a vortex distribution on the axis in Figure 2.4. The solution domain is scaled by time dependent stagnation pressure point offset, $z_c(t)$.

$$\begin{aligned} &\zeta = \zeta(\tau) = z/z_c(t) \\ &b(\tau) = z_b(\tau)/z_c(\tau) \\ &\text{The strength of the line vortex is in general as per Figure 2.4} \\ &\gamma(\zeta,\tau) = -2V_s(\zeta,\tau) \end{aligned} \tag{2.3}$$

Substituting definition of γ in Equation(2.3) into Equation(2.1) in V_n to solve w. Hence normal and tangential velocities are expressed in terms of vertical perturbation and the unkown $\gamma(\zeta)$ distribution.

$$\begin{aligned} V_n &= \frac{V + v + \frac{1}{2}\gamma \sin\beta}{\cos\beta} \\ V_s &= \frac{-1}{2}\gamma \end{aligned} \tag{2.4}$$

Free Sheet Dynamic Boundary Condition

Pressure Continuity: As per mathematical model in Figure 2.4 zero pressure starts beyond $z_c(t)$ which is now $\zeta = 1$:

$$C_p(\zeta,\tau) = 0 \quad \text{on} \quad \zeta \geq 1 \tag{2.5}$$

Using Bernoulli's Equation Vorus (1996) defined the non-dimensional pressure coefficient as:

$$C_p(\zeta,\tau) = V^2(\tau) - V_n^2(\zeta,\tau) - V_s^2(\zeta,\tau) + 2z_{c\tau}[\int_{\zeta_0=\zeta}^{b(\tau)} V_s(\zeta_0,\tau)\mathrm{d}\zeta_0 + \zeta V_s(\zeta,\tau)] + 2z_c[\int_{\zeta_0=\zeta}^{b(\tau)} V_{s\tau}(\zeta_0,\tau)\mathrm{d}\zeta_0 + b_\tau V_s(b,\tau)] \quad \text{on} \quad 0 \le \zeta \le 1 \tag{2.6}$$

and

$$C_p(\zeta,\tau) = 0 \quad \text{on} \quad 1 \le \zeta \le b(\tau) \tag{2.7}$$

to satisfy Equation(2.7), $V_n = 0$ for CUW and $V_n = V(\tau)$ for CW flow in Equation(2.6). Vorus differrentiated Equation(2.6) in ζ and C_p constant:

$$(V_s - z_{c\tau}\zeta)\frac{\partial V_s}{\partial \zeta} + z_c\frac{\mathrm{d}V_s}{\mathrm{d}\tau} = 0 \qquad 1 \le \zeta \le b(\tau) \tag{2.8}$$

This equation is to be satisfied by a vortex distribution on free sheet or jet head. It is nonlinear Euler's equation and one dimensional Burger's equation. Manupilating this further gives:

$$\begin{gathered} 0 = V^2(\tau) - V_n^2(\tau) - V_s^2(b,\tau) + 2(z_c b_\tau + z_{c\tau} b)V_s(b,\tau) \\ \text{with} \qquad z_{b\tau} = z_c b_\tau + z_{c\tau} b \end{gathered} \tag{2.9}$$

$$z_{b\tau} = \frac{V_s^2(b,\tau) + V_n^2(\tau) - V^2(\tau)}{2V_s(b,\tau)} \tag{2.10}$$

In Equation(2.10), $z_{b\tau}$ is the 'spray root velocity' or velocity of point B in Figure 2.3. $V_s(b,\tau)$ in Equation(2.10) is 'jet velocity' or velocity of fluid particle entering the jet at truncation point B. with coordinate $\zeta = b(\tau)$. V_n is specified as 0 or V by Equatio(2.2) for CUW and CW flow respectively. Equation(2.8) ensures that pressure is constant at free surface and Equatio(2.10) assures that the constant is zero.

Free sheet Vortex Distribution: The Equation(2.5) requires that a fluid particle, once deattached from the contour, retains its velocity while passing from cylinder contour into

free vortex sheet and then into the jet. Let's assume a particle gets seperated at τ', then its velocity at $z_c(\tau')$ will remain constant for all time $\tau > \tau'$ thereafter (Vorus 1996). Vorus developed a solution to Equation(2.8) in Galaen transformation of the intial and boundary conditions. This resulted in position of particles $\hat{\zeta}$ with velocities $V_s(\hat{\zeta}, \tau)$ as:

$$\hat{\zeta}(\zeta', \tau) = \frac{V_s(\zeta', \tau_0)(\tau - \tau_0) + z_c(\tau_0)\zeta'}{z_c(\tau)} \quad 1 \leq \zeta' \leq b(\tau_0), \tau \geq \tau_0 \tag{2.11}$$

$$\hat{\zeta}(\tau, \tau') = \frac{V_s(1, \tau')(\tau - \tau') + z_c(\tau')}{z_c(\tau)} \quad \tau \geq \tau' \geq \tau_0 \tag{2.12}$$

In Equation(2.11) τ_0 is starting time and is defined by user in the code. $V_s(\zeta', \tau_0)$ in $1 \leq \zeta' \leq b(\tau_0)$ is known from wedge similarity solution developed by Dobrovol'skaya (1969). This provides an initial condition. However, in future time steps, at $\tau' = \tau$, $\hat{\zeta}(\tau, \tau) = 1$, and $V_s(1, \tau)$ is unknown. Other $V_s(\hat{\zeta}, \tau)$ at respective $\hat{\zeta}(\tau, \tau')$ other than 1, which is the separation point, are known from previous time steps as explained above (Vorus 1996). Hence, as shown by Equation(2.10), Equation(2.11) and Equation(2.12), the outward advancement of the spray-root lags behind that of all particles in the jet at any time. Therefore except at $\zeta = 1$, the distribution of the vortex sheet is defined by Equation(2.11) and Equation(2.12).

Cylinder contour kinematic boundary condition

The kinematic boundary condition that is satisfies on the contour requires that there is no flow through the body surface.

$$V_n(\zeta, \tau) = 0 \quad \text{on} \quad 0 \leq \zeta \leq 1 \tag{2.13}$$

Substituting Equation(2.4) in Equation(2.13), the kinematic boundary condition becomes:

$$v(\zeta, \tau) + \frac{1}{2}\gamma(\zeta, \tau)\sin\beta = -V(\tau) \quad \text{on} \quad 0 \leq \zeta \leq 1 \tag{2.14}$$

Vorus further used Biot-Savart Law to eliminate $v(\zeta,\tau)$ in terms of $\gamma(\zeta,\tau)$ and further solved Equation(2.14). This γ is the vortex distribution on the cylinder contour and denoted by γ_c. Hence the equation obtained in (Vorus 1996) is:

$$\gamma_c(\zeta,\tau) = -\frac{2\cos\tilde{\beta}(\zeta,\tau)\zeta\kappa(\zeta,\tau)}{\sqrt{1-\zeta^2}}\left[V(\tau)+\frac{1}{\pi}\int_{s=1}^{b(\tau)}\frac{\gamma_s(s,\tau)\mathrm{d}s}{\kappa(s,\tau)\sqrt{s^2-1}}\right.$$
$$\left.+\frac{\zeta^2-1}{\pi}\int_{s=1}^{b(\tau)}\frac{\gamma_s(s,\tau)\mathrm{d}s}{\kappa(s,\tau)\sqrt{s^2-1}(s^2-\zeta^2)}\right] \quad \text{with} \quad \tilde{\beta}=\tan^{-1}(\sin\beta) \quad (2.15)$$

as per Vorus the value for $\kappa(\zeta,\tau)=1$ for constant dead-rise angle.

Velocity Continuity: 'Kutta condition' which is conservation of vorticity requires cylinder vorticity to approach the free sheet vorticity when ζ approaches 1. In the view of the non-singular character of $\kappa(\zeta,\tau)$ at $\zeta=1$ in Equation(2.15), in order to $\gamma_c(1)$ be finite, it is clearly necessary that the collectively singular terms in Equation(2.15) be zero as defined by Vorus (1996):

$$V(\tau)+\frac{1}{\pi}\int_{s=1}^{b(\tau)}\frac{\gamma_s(s,\tau)\mathrm{d}s}{\kappa(s,\tau)\sqrt{s^2-1}} \quad (2.16)$$

This provides relation a between the unknown functions $\gamma_s=-2V_s, z_{b\tau}$, and b.

Displacement Continuity: The specific requirement according to Figure 2.5 is $y_c(z_b,t)=y_s(z_b,t)$. In satisfying this requirement, the kinematic boundary condition in Equation 2.14, expressed dimensionally is (Vorus 1996):

$$v(\zeta,t)+\frac{1}{2}\gamma_c(\zeta,t)\sin\beta=-V(t) \quad \text{on} \quad 0\le z\le z_b(t) \quad (2.17)$$

The left hand side is clearly net vertical velocity of the fluid and must be equal to:

$$\frac{\partial y_c(z,t)}{\partial t}=-V(t)=v(\zeta,t)+\frac{1}{2}\gamma_c(\zeta,t)\sin\beta \quad \text{on} \quad 0\le z\le z_b(t) \quad (2.18)$$

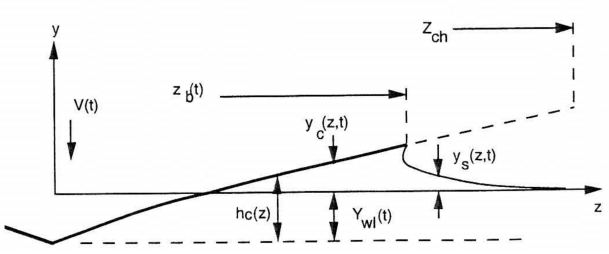

Figure 2.5: Displacement Continuity (Vorus 1996)

Vorus(1996) further solved the equations and expressed the in terms of cylinder countour γ_c:

$$\gamma_c^*(\xi,\tau) = -\frac{2\xi\cos\tilde{\beta}(\xi,\tau)}{\sqrt{1-\xi^2}}\left(\frac{1-\xi^2}{\xi^2}\right)^{\frac{\tilde{\beta}(\xi,\tau)}{\pi}}\left[Y_{wl}(\tau) - \frac{2}{\pi}\int_{s=0}^{1}\frac{\cos\tilde{\beta}(s,\tau)h_c\mathrm{d}s}{\kappa(s,\tau)\sqrt{1-s^2}} + \frac{2}{\pi}(1-\xi^2)\int_{s=0}^{1}\frac{\cos\tilde{\beta}(s,\tau)h_c\mathrm{d}s}{\kappa(s,\tau)\sqrt{1-s^2}(s^2-\xi^2)}\right] \quad (2.19)$$

Vorus then related free surface vortex distribution outside $z_b(t)$ to γ_c^* and using Biot-Savart law, giving free displacement distribution as:

$$y_s(\xi,\tau) = \frac{1}{2\pi}\int_{\xi_0=-1}^{1}\frac{\gamma_c^*(\xi_0,\tau)}{\xi_0-\xi}\mathrm{d}\xi_0 \quad (2.20)$$

In order to achieve displacement continuity, the singularity at $\xi_0 = \xi$ in Equation(2.20) must be removed. This is achieved in Equation(2.20) by zeroing the singular terms in displacement vortex strength in Equation 2.19, collectively (Vorus 1996). This can only be true if in Equation(2.19):

$$Y_{wl}(\tau) = \frac{2}{\pi}\int_{s=0}^{1}\frac{\cos\tilde{\beta}(s,\tau)h_c(s,\tau)\mathrm{d}s}{\kappa\ \ (s,\tau)\sqrt{1-s^2}} \quad (2.21)$$

Equation(2.21) provides a fourth relation between needed to determine four unknown function: $\gamma_s(\zeta,\tau), z_{b\tau}(\tau), b(\tau)$ and $z_c(\tau)$. After CW, $z_c(\tau)$ is known and constant as 1, and the displacement continuity by Equation(2.21) no longer applies.

Chapter 3

Discretization

The solution developed for the cylinder is time dependent and moves forward in discrete steps. At each step τ_i, where $i = 1, ...KK$ (KK is number of time steps defined by user), all three general continuity equations are satisfied. Hence, discrete formulations of these equations are needed to develop the computer code, i.e converting the continous integral functions to discrete algebriac equations for the purpose of computation.

3.1 Displacement Continuity

Vorus (1996) used the displacement continuity condition 2.21 for CUW flow to eliminate $\Delta\tau_i$, which is possible because in Vorus' original work z_{ci} is defined. However, in the current work. the time step ('dt') is an user input and converted to $\Delta\tau_i$. z_{ci} is calculated rather than defined by user. Hence, the discretized form of Equation(2.21) is:

$$Y_{wli} = \frac{2}{\pi} z_{bi} \cos\tilde{\beta} \tan\beta \quad \text{for constant deadrise angle} \quad \kappa = 1 \quad h_c = z_b s \tan\beta \tag{3.1}$$

The 'wetting factor' or 'jet-rise' was originally defined by Wagner (1932). Wagner obtained the wetting factor offset as $\frac{\pi V_0 t}{2\tan\beta} = \frac{\pi}{2}$ in his linearized model. With this the wetting factor gets the definition as the ratio of the spray-root ordinate above the wedge apex, to the height of the undisturbed free surface above the apex. Vorus(1996) redefined the wetting factor as:

$$WF = \frac{\pi\sqrt{\pi}}{b\Gamma(\lambda)\Gamma(\frac{3}{2}-\lambda)\cos\tilde{\beta}} \quad \text{and} \quad \lambda = \frac{1}{2} - \frac{\tilde{\beta}}{2} \tag{3.2}$$

In Equation(3.2) Γ is Gamma function according to I.S.Gradshteyn and Ryzhik (1965). Hence definition of wetting factor is used to compute z_{bi} by:

$$Y_{wli} = Y_{(wli-1)} + V_i \Delta\tau_i \tag{3.3}$$

$$\begin{aligned} z_{bi} \tan\beta &= WF * Y_{wli} \\ z_{bi} &= \frac{Y_{wli}\pi\sqrt{\pi}}{b\Gamma(\lambda)\Gamma(\frac{3}{2}-\lambda)\cos\tilde{\beta}\tan\beta} \end{aligned} \tag{3.4}$$

Now z_{ci} is calculated by:

$$z_{ci} = \frac{z_{bi}}{b_i} \tag{3.5}$$

The values for V_i and b_i are guessed from previous time step. The complete explanation and order of equations used are explained in chapter 4.

In CW flow, the displacement continuity is disregarded as z_{ci} ceases to advance further and is fixed to 1 as discussed in Section 2.1.2. Hence, only Equation(3.3) is used and from Equation(3.5):

$$z_{bi} = b_i \tag{3.6}$$

3.2 Pressure Continuity

As discussed in Section 2.1.2, a zero pressure condition is satisfied by Equations(2.10), (2.11), and (2.12). $\hat{\zeta}$ in (2.11) and (2.12) gives the absolute position of fluid particles at time τ having passed through $\zeta = 1$ at their respective previous time steps. Hence the particle position distribution is constructed as shown in Figure 3.1 using:

$$\hat{\zeta}_j = \frac{V_{si-j}(\tau_i - \tau_{i-j}) + z_{ci-j}}{z_{ci}} \quad \text{with} \quad j = 1, ..., i \tag{3.7}$$

The velocity V_{si0} at $\hat{\zeta}_0 = 1$ in Figure 3.1 is usually unknown and is initially guessed

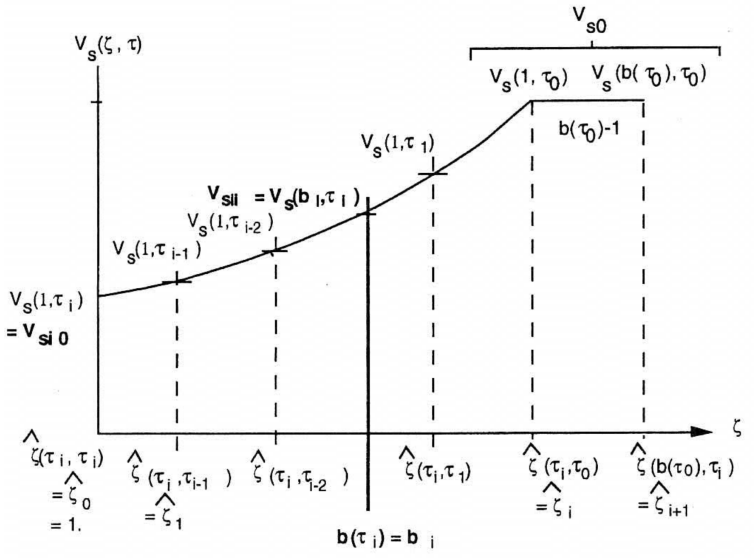

Figure 3.1: Particle position in free sheet (Vorus 1996)

from the previous time step and later solved using velocity continuity as discussed in next Section 3.3. After development of the particle distribution, velocity of fluid particle, V_{sii} at $\hat{\zeta} = b_i$ in Figure 3.1 is calculated using interpolation. This V_{sii} is required to compute $z_{bi\tau}$ in Equation(2.10). The *free vortex sheet* is then overlaid over the velocity distribution however, truncated at b_i, to find the vortex strength distribution in the free surface except at $\zeta = 1$. The free vortex sheet is developed in time and is between $\zeta = 1$ to $\zeta = b_i$. It is discretized into small segments so that the vortex strength over it remains constant as shown in Figure 3.2. n_i is the number of elements in free sheet between $\zeta = 1$ and $\zeta = b_i$ at particular time step. For convenience $n_i = i$, i.e for the first time step, there will be one vortex element or for the second time step there will be two vortex elements and so on. In general, a new segment is added at every time step and the sheet is re-discretized every time. The length of segments is defined as ζ_{ij} by:

$$\zeta_{ij} = 1 + \sum_{k=1}^{j} \delta b_{ik} \equiv \zeta_{ij-1} + \delta b_{ij} \quad \text{with} \quad j = 1, ...n_i \tag{3.8}$$

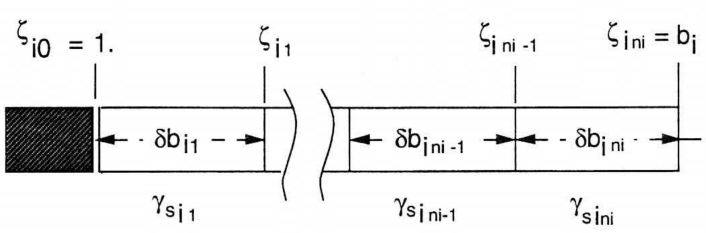

Figure 3.2: Vortex Sheet Development (Vorus 1996)

with

$$\delta b_{ij} = \frac{\delta z_{b_{n_i-j+1}}}{z_{ci}} \quad \text{with} \quad \delta z_{bi} = (z_{bi\tau} - z_{ci\tau})\Delta\tau_i \tag{3.9}$$

$z_{ci\tau}$ is calculated using:

$$z_{ci\tau} = \frac{z_{bi\tau} - z_{ci}(\frac{b_i - b_{i-1}}{\Delta\tau_i})}{b_i} \tag{3.10}$$

Now the positions of ζ_{ij} are defined at a particular time step with $\zeta_{i0} = 1$ and $\zeta_{in_i} = b_i$ as in Figure 3.2 in the free vortex sheet.

3.3 Velocity Continuity

After defining the positions of particles on the free sheet, the vortex strengths need to be defined. As discussed in Section 3.2 the vortex strengths are constant over the element length and evaluated at ζ_{ij} and averaged to apply at the segment mid point, $\bar{\zeta_{ij}}$. The strengths of these vortices are $\gamma_{sij} \equiv -2V_s(\bar{\zeta_{ij}}, \tau_i)$ (Vorus 1996). However, Savander et al. (2002) pointed out that "***differentiation of potential, ø, in z-direction should yield*** w ***instead of*** v_s" during mathematical modeling as in Figure 2.4. Hence Vorus fixed the problem in his original work and re-defined the vortex strengths as:

$$\gamma_{sij} = 2V_i \sin\beta - V_s(\bar{\zeta_{ij}}, \tau_i) \tag{3.11}$$

The velocity of fluid particles $V_s(\zeta_{ij}, \tau_i)$, in the sheet is calculated by interpolation between $\zeta = 1$ and $\zeta = b_i$ using calculated V_{sii} and guessed V_{si0} at each ζ_{ij} for every time step and

averaged out to apply at the mid section as $V_s(\bar{\zeta_{ij}}, \tau_i)$.

The velocity continuity condition at $\zeta = 1$ is achieved by satisfying Equation(2.16). The discretized version of same can be written as:

$$0 = V_i + \frac{1}{2\pi\bar{\lambda_i}} \sum_{j=1}^{n_i} \frac{\gamma_{sij}}{\kappa_{ij}} (T_{ij} - T_{ij-1}) \quad \kappa_{ij} = 1 \tag{3.12}$$

with

$$T_{ij} = (\zeta_{ij}^2 - 1)^{\bar{\lambda_i}} F(\bar{\lambda_i}, \bar{\lambda_i}, \bar{\lambda_i} + 1; 1 - \zeta_{ij}^2) \tag{3.13}$$

The function F in Equation(3.13) is the hypergeometric function of argument $1-\zeta_{ij}^2$ (I.S.Gradshteyn and Ryzhik 1965). Now Equation(3.12) is used to calculate γ_{si1} which is further used to compute V_{si0} by Equation(3.11).

3.4 Cylinder pressure and Force distribution

Equation(2.6) gives the general contour of dimensionaless pressure coefficient distribution. Substituting Equation(2.8) and Equation(2.9) gives at any τ_i:

$$\begin{aligned} C_{pi}(\zeta) = \frac{1}{4}[\gamma_{ci}^2(1) - \gamma_{ci}^2(\zeta)] - z_{ci\tau} \int_{\zeta_0=1}^{1} \gamma_{ci}(\zeta_0) \mathrm{d}\zeta_0 + \\ z_{ci\tau} \Big[\zeta\gamma_{ci}(\zeta) - \gamma_{ci}(1)\Big] - z_{ci} \int_{\zeta_0=1}^{1} \gamma_{ci\tau}(\zeta_0) \mathrm{d}\zeta_0 \end{aligned} \tag{3.14}$$

where, $\gamma_{ci\tau} = \frac{\gamma_{ci} - \gamma_{ci-1}}{\Delta\tau_i}$.

This requires non-singularity in vortex distribution on the contour, hence Equation(2.15) can be discretized as:

$$\gamma_{ci}(\zeta) = \bar{\kappa_i}(\zeta) \sum_{j=1}^{n_i} \frac{\gamma_{sij}}{\bar{\kappa_{ij}}} [S_{ij}(\zeta) - S_{ij-1}(\zeta)] \quad 0 \le \zeta \le 1 \qquad \text{with} \quad \kappa_i = 1 \tag{3.15}$$

In Equation(3.15):

$$S_{ij}(\zeta) \equiv \frac{\cos\tilde{\beta}(\zeta)}{\pi\bar{\lambda}_i} Q_{ij}(\zeta)^{\bar{\lambda}_i} F[\bar{\lambda}_i, \bar{\lambda}_i, \bar{\lambda}_i + 1; Q_{ij}(\zeta)] \tag{3.16}$$

with

$$Q_{ij}(\zeta) \equiv \frac{\zeta^2(\zeta_{ij}^2 - 1)}{\zeta_{ij}^2 - \zeta^2} \tag{3.17}$$

Once the $\gamma_{ci}(\zeta)$ distribution is calculated. Equation(3.14) is solved using Simpson's first integration rule to get $C_{pi}(\zeta)$ distribution. The non-dimensional force coefficient is defined as (Vorus 1996):

$$C_{fi} \equiv \frac{f_i}{\rho V_0^2 Z_{ch}} = z_{ci} \int_{\zeta=0}^{1} C_{pi}(\zeta) \mathrm{d}\zeta \tag{3.18}$$

Equation(3.18) is also solved using Simpson's first integration rule to compute the non-dimensional force coefficient.

For free-fall, the velocity varies in time and is calculated at every time step after the computation of C_f. C_f is a non-linear function of V_i, hence an outer iteration loop is required. To calculate V_i Newton's Second law is applied to the wedge free body and acceleration, $\dot{V}_i$, is calculated as:

$$\dot{V}_i = \frac{G - (C_{fi} + C_b)}{C_m} \tag{3.19}$$

where, C_b is buoyant force coefficient, G is non-dimensional gravity, $\frac{gZ_ch}{V_0^2}$, C_m is mass coefficient defined as $\frac{W}{\rho g Z_{ch}^2}$, and W is weight per length.

Finally, the velocity (V_i) for that time step is calculated by:

$$V_i = V_{i-1} + \dot{V}_i \Delta\tau_i \tag{3.20}$$

Chapter 4

Computation

4.1 Algorithm Explained

4.1.1 Chine-Unwetted

The code reads inputs defined by user. The discretization for the contour of interest is user dependent. The first step is to discretize the contour which is done by *spread* subroutine developed by Dr. William S. Vorus. According to (Zhao and Faltinsen 1993) the boundary value problem can be considered to be linear for the impact of a symmetric cylinder contour. Vorus further mentioned that the similarity solution exists in the initial time period of impact, which solves the initial condition (Vorus 2017). This can also be considered as $i = 0$ for $\tau_0 = \Delta t$. At the end of it, the solution parameters available are τ_0, b, V_i, V_{s00}, which forms the initial guess for the next time step i.e $i = 1$.

Now for further time steps, nested iteration loops of non-linear equations are solved with the help of three concentric loops. The outermost loop computes the wedge velocity V_i required in Equation(3.3), (3.11), (3.12) and (3.20). The next inner loop solves for V_{si0} using Equations(3.11) and (3.12). The inner most loop solves for b_i in Equations(3.4), (3.5), (3.8), (3.9) and (3.10). For simplicity $i = 1$ is solved separately and then the outermost loop, containing the three loops mentioned above, keeps the count for further time steps ($i = 2...$). The solution procedure at each time steps is as follows:
A trial iterate of $V_i = V_{i-1}$, $V_{si0} = V_{s(i-1)0}$, $b_i = b_{i-1}$ is set as first guess. The program goes to inner most loop where Y_{wli} is computed using Equation(3.3) by guess velocity and previous

calm water draft. z_{bi} and z_{ci} are computed using Equations(3.4) and (3.5) respectively with help of guess b_i. The next step is to find velocity distribution of particles as per Figure 3.1. This is done using Equation(3.7). With the help of particle distribution ($\hat{\zeta}$) and their respective velocity at that location as per Section 2.1.2, the code finds the two positions i.e $\hat{\zeta}$ between which guess b_i lies. Then the velocity at that b_i, V_{sii}, is calculated using interpolation between those two $\hat{\zeta}_j$. This V_{sii} is used to calculate $z_{bi\tau}$ in Equation(2.10) which further is used to compute $z_{ci\tau}$ using Equation(3.10).

The free vortex sheet is re-discretized at every time step and the number of discretization is equal to numerical value of the time step. $z_{ci\tau}$ and $z_{bi\tau}$ are used to calculate each segment length of free sheet vortex distribution using Equations(3.9) and (3.10). The positions of the free vortex sheet particles are stored as ζ_{ij} using Equation(3.8). The last ζ_{ij} theoretically should be equal to b_i, which forms the check condition criteria for the inner most loop iteration. If the difference between ζ_{ii} and b_i is more than critical value, then b_i is changed using the Newton-Raphson iteration scheme. If the value is within critical range defined by the user, the first iteration loop is exited and the value is b_i is found and set.

The middle loop then takes the current values of b_i, free sheet vortex distribution, ζ_{ij} and guessed V_{si0} to calculate the vortex strengths at every ζ_{ij}. The velocities of each vortex at respective ζ_{ij} are calculated using interpolation between guessed V_{si0} and calculated V_{sii} values. These velocities are further averaged to apply at the midpoints of the segments, and they are converted into vortex strength at every position γ_{ij} using Equation(3.11), where $i =$ *time step number* and $j = 1, 2.., i$. Using Equations(3.12) and (3.13), γ_{i1} is updated and a new V_{si0} is found using Equation(3.11). This new calculated value of V_{si0} is compared with the guessed V_{si0}. If the difference is more than a critical value, then the value of V_{si0} is updated and all calculations above including the inner most loop repeated until the value of V_{si0} and b_i are once again set. Once these values are obtained, the program exits the middle loop and comes to the outer loop where contour vortex strength γ_{ci} is computed using Equations(3.15) to (3.16). γ_{ci} is required to compute pressure coefficients $C_{pi}(\zeta)$ along the contour using

Equation(3.14). Once $C_{pi}(\zeta)$ is calculated, it is used to determine dimensionaless force coefficient C_{fi} using Equation(3.18). This force coefficient give dimensionaless acceleration via Equation(3.19) which further yields velocity at the current time step by Equation(3.20). The calculated velocity is compared with the guessed velocity V_i. If the difference is more than critical value, the guessed velocity is updated and all calculations are repeated including the two inner loops. If the difference has fallen below critical value, we have all the quantities needed at a particular time step and the program moves to the next time step. The calculated values b_i, V_{si}, V_i become the guessed value for the next time step. Figure 4.1 depicts the sequential solution of non-linear equations solved at each time step to achieve the desired parameters.

4.1.2 Chine-Wetted

At the end of each time step the code checks the value of z_{ci}. If $z_{ci} = 1$, the code jumps to chine wetted part where the calculations for that particular time step and further time steps are performed in the same manner as explained in Section 4.1.1 and shown in Figure 4.1. The only changes made are: there is no further advancement of zero pressure offset, $z_{ci} = 1$ (Vorus 1996), hence $z_{ci\tau}$ is zero and $z_{bi} = b_i$ by Equation(3.6). Equation(2.10) is used to calculate $z_{bi\tau}$ in inner most loop, but the value of V_n is V_i instead of 0 for CW calculations (Vorus 1996). The remaining variables are calculated in exactly the same manner as in Section 4.1.1. The code exits the time step loop when $V_i = 0$ as the flow physics fails after the wedge reverses its direction because of buoyant force (Savander et al. 2002).

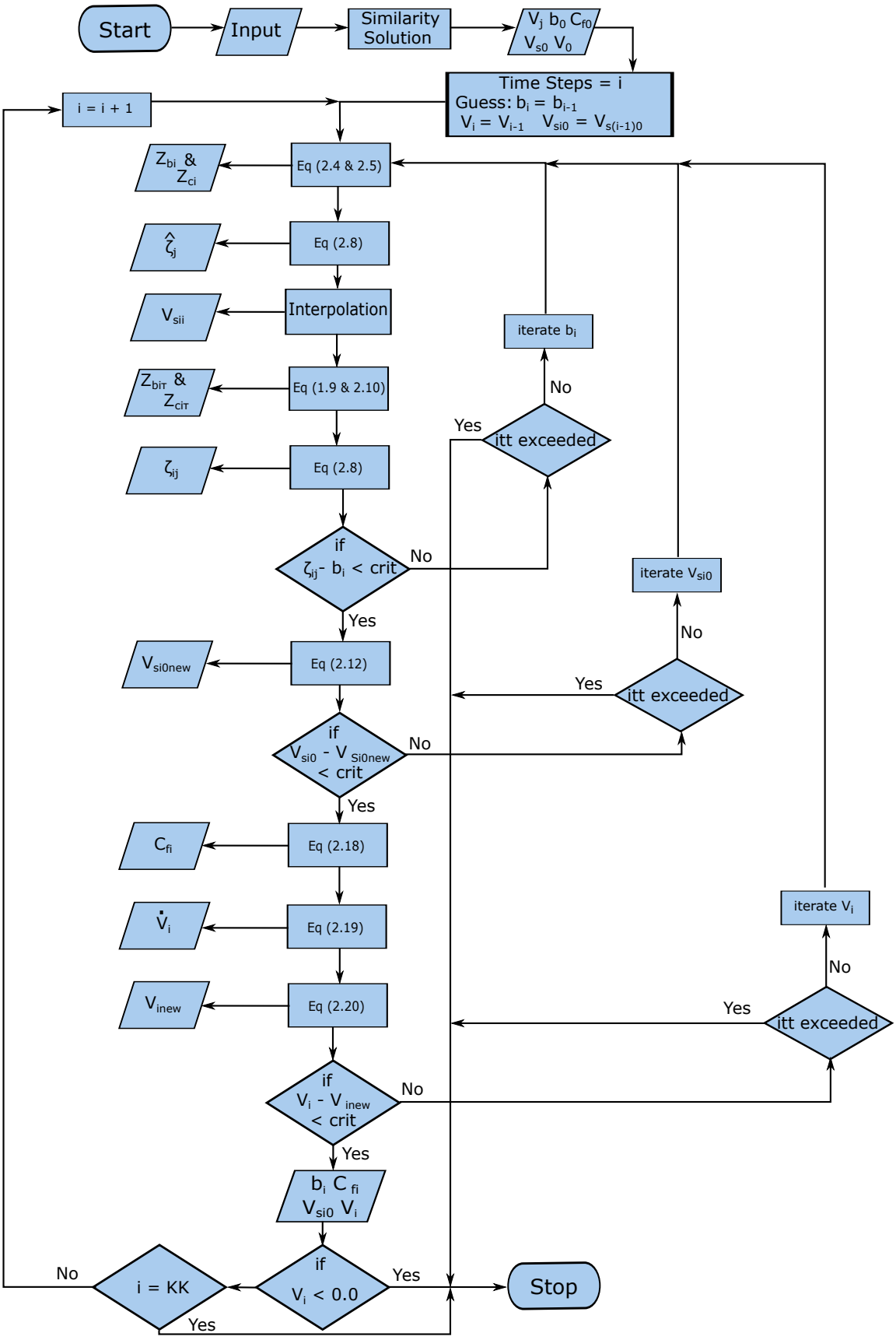

Figure 4.1: Flowchart

Chapter 5

Discussion and Results

5.1 Validation

The code developed is verified with Vorus (1996) data as shown in Figures 5.4 to 5.10. As per Table 5.1, the code is validated using *Constant Impact velocity*, $Free-Fall$ *with* $C_m = 0.3$ *and* 0.5. The principal parameters plotted in Figure 5.4 are $z_b(\tau)$, $z_c(\tau)$ and $V_s(1,\tau)/10$ for constant impact velocity. Since the impact velocity does not change throughout the time domain, the outer-most loop of the code that iterates on V_i, is skipped. Figure 5.5 and Figure 5.6 are plots for keel pressure and non-dimentionalized force coefficient. Transition from CUW to CW flow is clearly seen as large negative gradient of V_s on commencement of CW flow in Figure 5.4. The code runs until the non-dimentionalized time(τ) is 1. This is to overlay the predicted data on (Vorus 1996) data. As shown in Tables 5.2, 5.3 and 5.4, the parameters are compared at three different times, at CUW, commencement of CW and CW phase for each of three different scenarios. There is a 14.7% difference during CUW phase in V_s. This difference and other differences can be explained because of difference in (Vorus 1996) as pointed out by (Savander et al. 2002) in Section3.3. This code uses new definition of γ as per Equation(3.11). To verify the working of code more, the definition of γ was changed back according to Equation(2.3) and executed for $C_m = 0.3$ and $C_m = 0.5$. As shown in Figure 5.9 and Figure 5.10, the predicted data is very similar to Vorus' data. As expected the heavier wedge reaches CW first. The Table 5.3 and Table 5.4 compares the data predicted by old definition of γ .vs. new definition of γ. It can be easily observed the %difference reduces with increase in impact velocity as also explained in Section 5.2.

Table 5.1: Scenarios for Validation

Parameters	Constant Velocity	Free Fall	Free Fall
G	-	0.1	0.1
C_M	-	0.3	0.5
Z_{ch} [m]	0.125	0.125	0.125
Impact Velocity [m/s]	3.5	3.5	3.5

Table 5.2: Constant Velocity Comparison at $\tau = 0.15$, 0.27, and 0.7

Time τ	Parameters	Vorus	Code	% Difference
0.15	$V_s(\tau)$	0.761	0.874	14.7
	$Z_b(\tau)$	0.547	0.564	3.0
	$Z_c(\tau)$	0.547	0.564	3.0
	$C_p(0,\tau)$	7.456	5.385	-27.7
	C_f	3.9	4.09	4.8
0.27	$V_s(\tau)$	0.337	0.328	-2.6
	$Z_b(\tau)$	1.000	1.040	4.0
	$Z_c(\tau)$	1.000	1.000	0.0
	$C_p(0,\tau)$	7.456	5.385	-27.7
	C_f	8.872	7.660	-13.6
0.7	$V_s(\tau)$	0.108	0.141	30.5
	$Z_b(\tau)$	1.450	1.540	6.2
	$Z_c(\tau)$	1.000	1.000	0.0
	$C_p(0,\tau)$	1.129	0.868	-23.1
	C_f	0.714	0.633	-11.4

The code predicts the impact velocity within 8% of difference as compared old definition. Even though the difference is as high as 35% at some places, Table 5.4 for V_s, the absolute values and difference between them is very small, i.e to first or second decimal place. Overall the computed parameters agree with theory and previous data by (Vorus 1996). Hence the code gives reliable values. The certain differences are because of simple iteration scheme used rather than more accurate iteration schemes. The use and testing of different iteration schemes is itself a humongous task. The difference in V_s at time zero is because, according to (Zhao and Faltinsen 1993) wedge similarity solution exits in the very initial phase of impact, hence the similarity solution created by (Vorus 2017), needs an iterative scheme even though its results are just forming an initial guess of values for the first time step.

Table 5.3: Free-Fall Velocity Comparison $C_m = 0.3$ at $\tau = 0.2$, 0.6, and 0.7

Time τ	Parameters	Vorus	Old γ	New γ	Old Difference(%)	New Difference(%)
0.2	$Z_c(\tau)$	0.509	0.542	0.578	6.4	13.5
	$Z_b(\tau)$	0.509	0.545	0.580	7.0	13.9
	$V_s(\tau)$	0.784	0.780	0.924	-0.5	17.8
	$V(\tau)$	0.509	0.489	0.529	-3.9	3.9
0.6	$Z_c(\tau)$	1.000	0.988	1.000	-1.2	0.0
	$Z_b(\tau)$	1.002	0.999	1.073	-0.2	7.0
	$V_s(\tau)$	0.340	0.322	0.240	-5.4	-29.5
	$V(\tau)$	0.220	0.205	0.246	-6.9	11.4
0.7	$Z_c(\tau)$	1.000	1.000	1.000	0.0	0.0
	$Z_b(\tau)$	1.057	1.039	1.110	-1.7	5.0
	$V_s(\tau)$	0.089	0.104	0.109	16.8	22.4
	$V(\tau)$	0.205	0.186	0.204	-9.2	-0.5

Table 5.4: Free-Fall Velocity Comparison $C_m = 0.5$ at $\tau = 0.2$, 0.46, and 0.7

Time τ	Parameters	Vorus	Old γ	New γ	Old Difference(%)	New Difference(%)
0.2	$Z_c(\tau)$	0.578	0.586	0.627	1.3	8.4
	$Z_b(\tau)$	0.579	0.598	0.637	3.2	9.9
	$V_s(\tau)$	0.900	0.900	1.080	0.0	20.0
	$V(\tau)$	0.579	0.579	0.621	-0.06	7.1
0.46	$Z_c(\tau)$	1.000	1.000	1.000	0.0	0.0
	$Z_b(\tau)$	1.002	1.002	1.060	0.0	5.7
	$V_s(\tau)$	0.493	0.320	0.216	-35.0	-56.2
	$V(\tau)$	0.322	0.316	0.390	-1.8	21.1
0.7	$Z_c(\tau)$	1.000	1.000	1.000	0.0	0.0
	$Z_b(\tau)$	1.136	1.131	1.202	-0.5	5.7
	$V_s(\tau)$	0.112	0.105	0.125	-6.2	11.6
	$V(\tau)$	0.296	0.272	0.340	-8.1	14.8

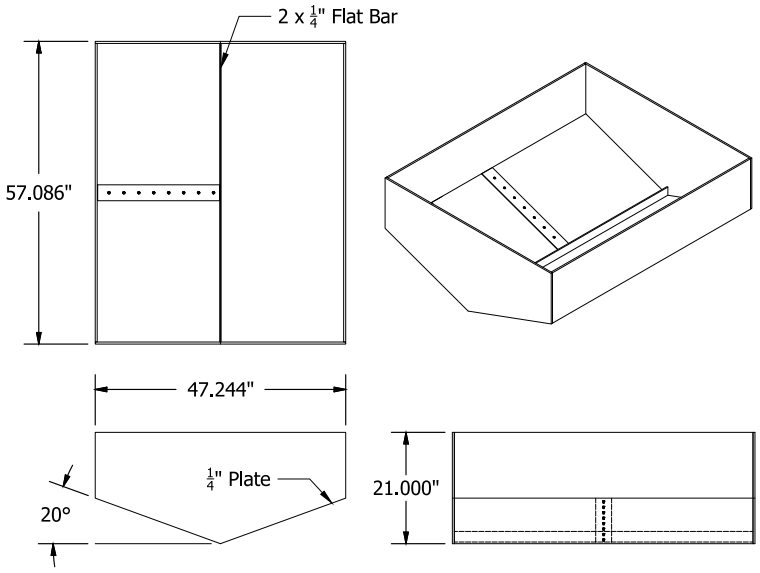

Figure 5.1: Aluminum Wedge (Eastridge 2017)

Table 5.5: Wedge Specification

Weight/Length [N/m]	1264
Breadth [m]	1.200
Length [m]	2.133
Dead rise angle [deg]	20

5.2 Experiments And Numerical Predictions of Pressure Coefficient

The model in consideration for the experimentation is an aluminum wedge as shown in Figure 5.1 with the specifications as in Table 5.5 Figure 5.2 shows the experimental setup for the wedge experiments in the towing tank at the University of New Orleans. The wedge was dropped from four different drop heights $0.1524meter$, $0.3048meter$, $0.4572meter$ and $0.6096meter$ leading to four different impact velocities $1.467m/s$, $2.0693m/s$, $2.5551m/s$ and $2.9693m/s$ respectively. The wedge had eight pressure sensors along the bottom plate from keel to chine located at positions, $0.0293m$, $0.1009m$, $0.1725m$, $0.2441m$, $0.3157m$, $0.3873m$, $0.4590m$ and $0.5306m$ from the keel as shown in Figure 5.3. The pressure readings acquired from the respective pressure sensor were non-dimentionalized on $\frac{1}{2}\rho V_0^2$ and overlay-ed on

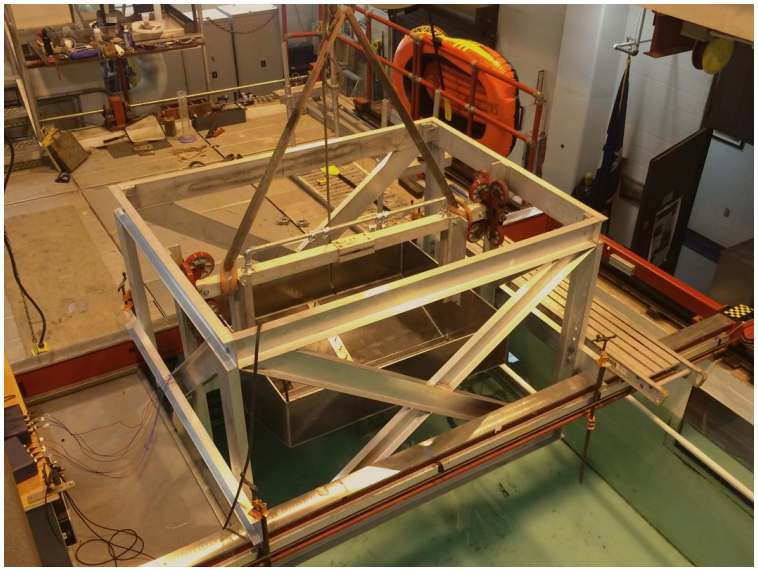

Figure 5.2: Experimental Setup

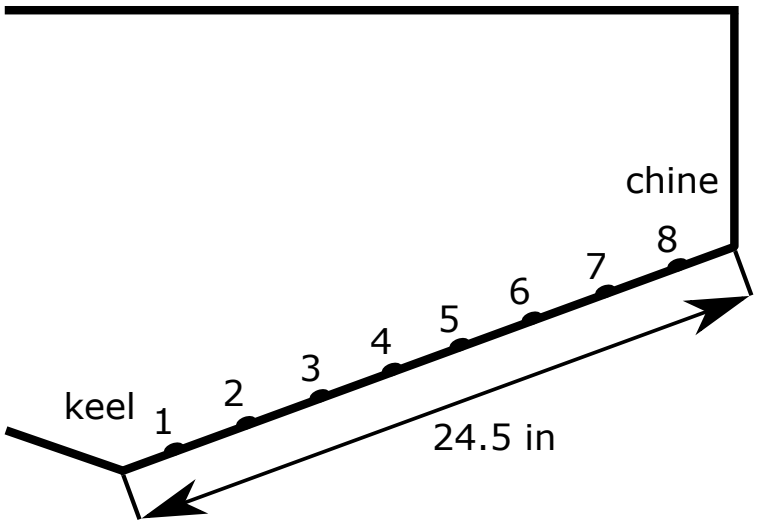

Figure 5.3: Location of pressure sensors across the wedge

numerically predicted, $C_p(\zeta, \tau)$, at the same locations as sensors as shown in Figure 5.15 to Figure 5.46. The pressures were plotted against non-dimentionalized time(τ). Numerical solution parameters are also plotted from Figure 5.11 to Figure 5.14 for respective heights. The only experimental data overlay-ed is the non-dimentionalized velocity(on impact velocity). There were no other means to measure the parameters such as V_s, $z_b(\tau)$ and $z_c(\tau)$, hence the practicality of code will confirm the values of these parameter. It is clearly evident from Figure 5.11 to Figure 5.46 that the numerical computed time at which chine gets wet agrees with experimental chine wetting time. This also validates the practicality of code. However, the code only predicts the pressure when that particular position gets wet but the sensor reads pressure before the location gets wet. This happens because during the fall and impact, the plate vibrates which causes noise in the sensor, this phenomenon becomes more evident on moving away from keel. The plate is less stiff towards the chine than it is near to the keel. As seen from Figure 5.11 to Figure 5.14 the chine wetting comes earlier for lower drop height. The predicted velocity is higher than the measured velocity, however right after impact there is an increase in velocity measured while the increase in velocity predicted is not that much. This is due to the iteration procedure incorporated as well as the tolerance between guessed and calculated values. The iteration procedure for the velocity uses Barrycentric combination of difference calculated between guessed and iterated values until the calculated value is within the tolerance.

It is because of this difference in the calculated velocity and measured velocity there is a difference in calculated and measured pressure. The code solves the impact problem in two dimensions for now, hence consider the wedge to be infinitely long, but in experimentation the wedge has finite length. It was observed during experiments that the water rushes out from the fore and aft ends of the wedge as it impacts the water. This three dimensional effect is not yet accounted in the code. This also accounts for the difference in numerical and experimental values. Immediately after the impact, the measured pressure at $0.0293m$ and $0.1009m$ from the keel is higher than the numerical pressure as seen in Figure 5.15 to 5.46, .

Table 5.6: Peak Pressure comparison for impact velocity $1.466m/s$

Numerical	Experimental	% Difference
14.762	24.276	-39.1
16.270	24.253	-32.9
16.770	13.716	22.2
15.740	11.359	38.5
13.500	11.096	21.6
11.290	9.162	23.2
9.660	6.681	44.5
8.020	3.488	129.8

This is because the change measured velocity is higher and more positive than the numerical velocity as seen in Figures 5.11 to 5.14. As the jet spray-root moves further towards the chine, the predicted pressures start to increase higher than the measured because of the difference in numerical and measured velocity. It is observed that from position $0.1725m$ to $0.3157m$ the percentage difference reduces because both velocities are almost close to each other. There is drop in pressure observed in numerical data exactly at the chine wetting. This is because of discontinuity at the hard chine. The singularity is an inverse square root and is integrable over pressure integration. However, the singularity still gives large unexpected values of pressure and force at the chine because of the discretization. One has to make sure the forces do not exceed the breaking or yielding limit of the material used. The negative pressure coefficients after chine wetting is due to the difference in measured and numerical velocities, and numerical velocities having greater negative gradient than measured. It is observed that the difference is reduced at higher drop heights as seen in Table 5.6 to Table 5.9. Also with increase in discretization of the contour, the numerical pressures come close to the measured pressure; however, the iteration procedure for velocities also needs to be improved, keeping the computational capacity in mind.

Table 5.7: Peak Pressure comparison for impact velocity $2.069 m/s$

Numerical	Experimental	% Difference
13.938	20.765	-32.8
15.036	19.813	-24.1
15.241	12.308	23.8
13.645	12.039	13.3
11.633	10.420	11.6
9.355	9.162	2.1
7.537	6.786	11.0
6.202	3.655	69.6

Table 5.8: Peak Pressure comparison for impact velocity $2.555 m/s$

Numerical	Experimental	% Difference
16.920	21.471	-21.1
15.880	20.399	-22.1
15.105	10.726	40.8
12.695	11.268	12.6
10.185	8.367	21.7
8.126	6.540	24.2
6.305	4.959	27.1
5.222	3.081	69.4

Table 5.9: Peak Pressure comparison for impact velocity $2.969 m/s$

Numerical	Experimental	% Difference
14.526	20.010	-27.4
16.050	19.619	-18.1
14.765	10.587	39.4
12.247	10.897	12.3
9.638	7.951	21.2
7.624	6.346	20.1
5.893	3.425	72.0
4.774	2.943	62.1

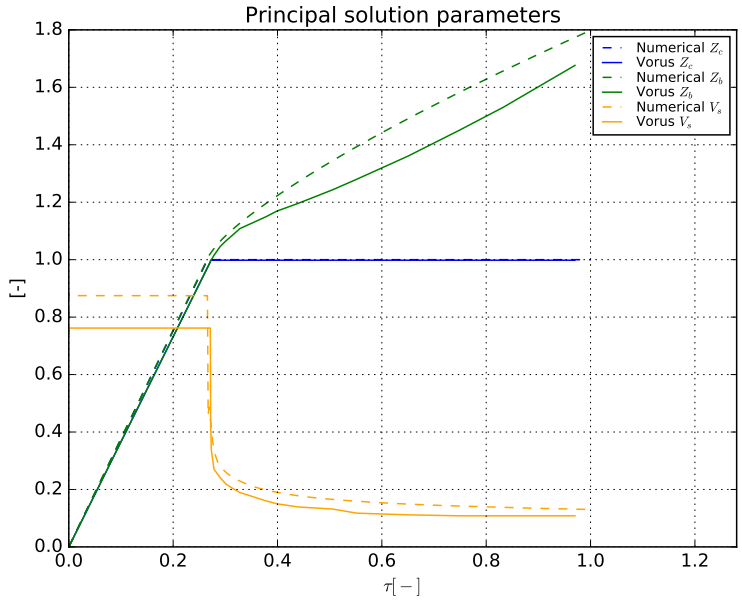

Figure 5.4: Principal Solution Parameters: constant velocity impact

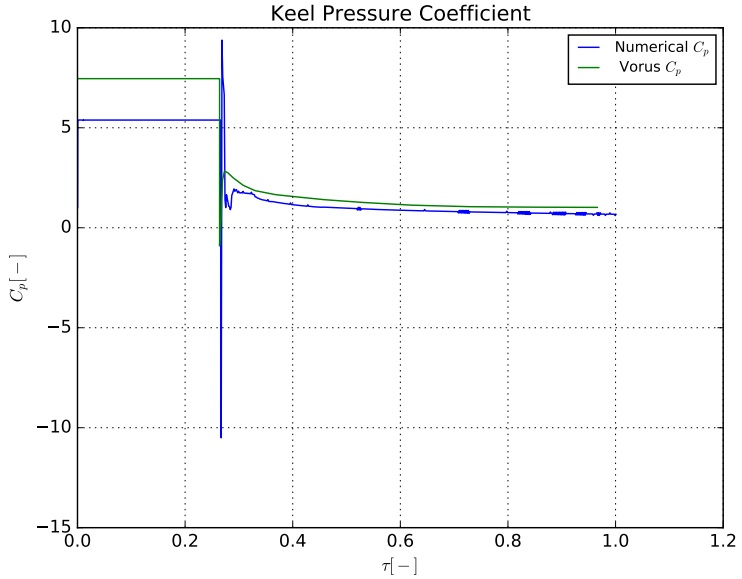

Figure 5.5: Keel Pressure Coefficient, $C_p(0, \tau)$

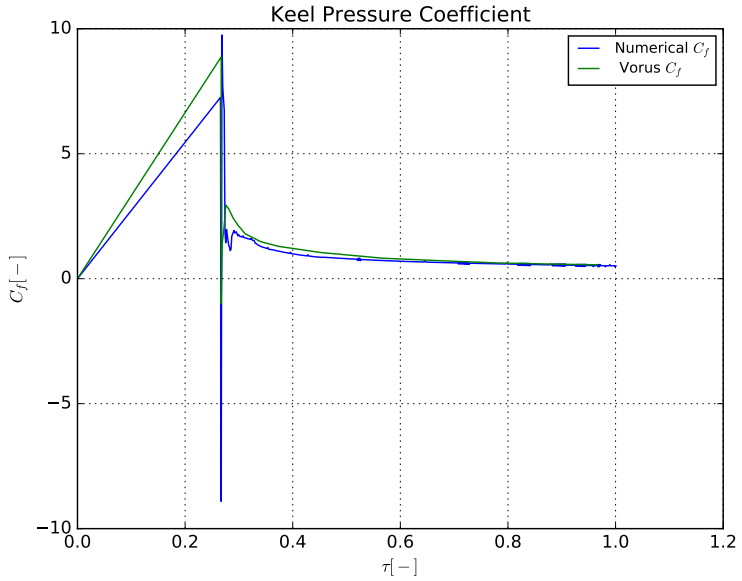

Figure 5.6: Pressure Force Coefficient, C_f

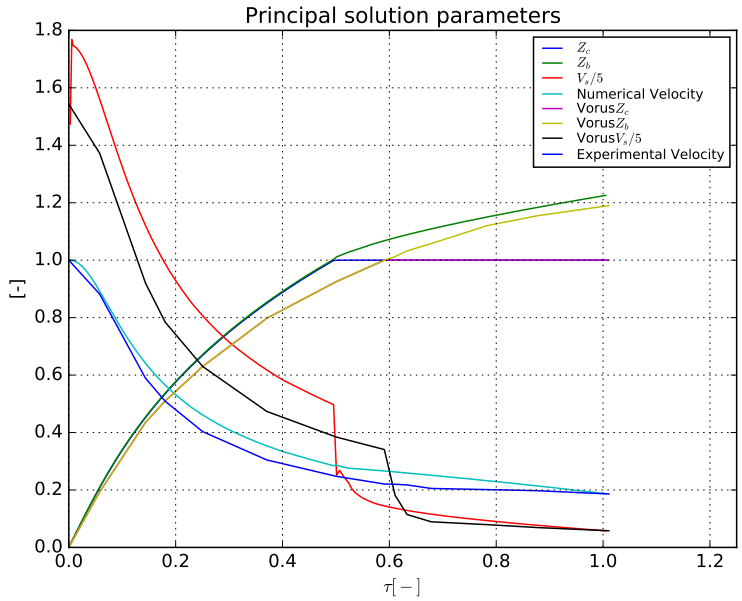

Figure 5.7: Principal Solution Parameters: $C_m = 0.3$

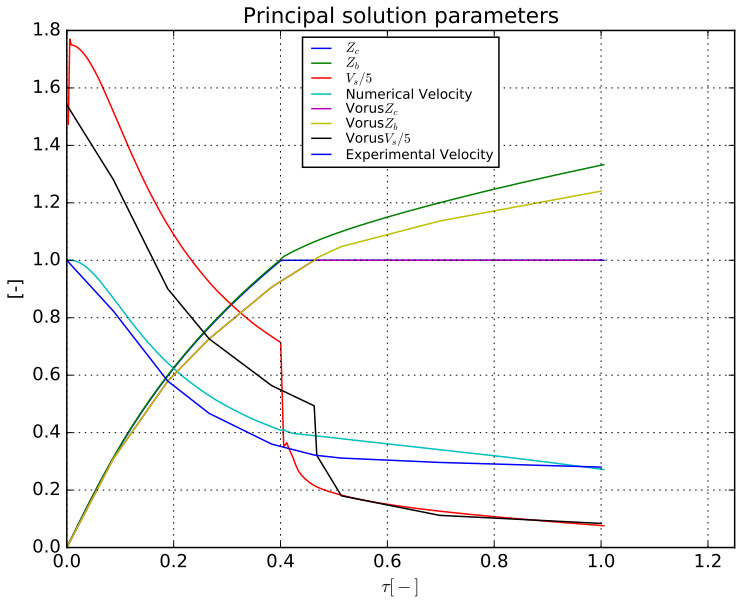

Figure 5.8: Principal Solution Parameters: $C_m = 0.5$

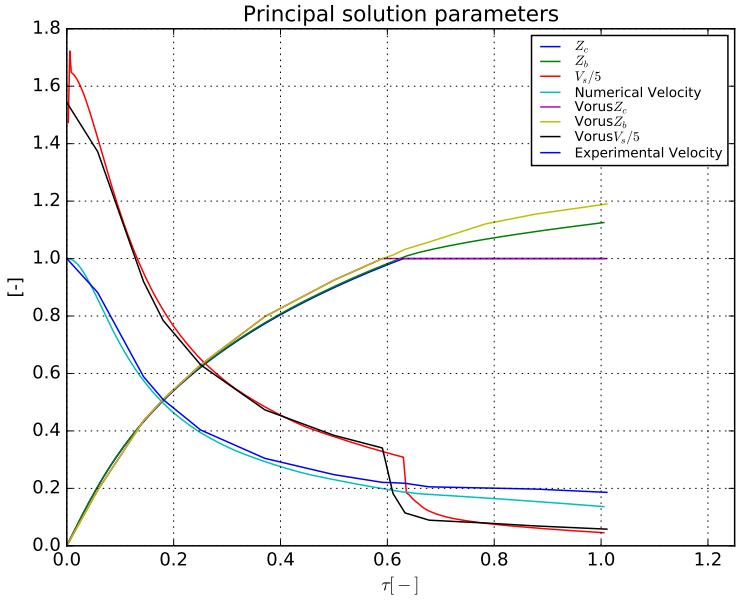

Figure 5.9: Principal Solution Parameters with old γ definition: $C_m = 0.3$

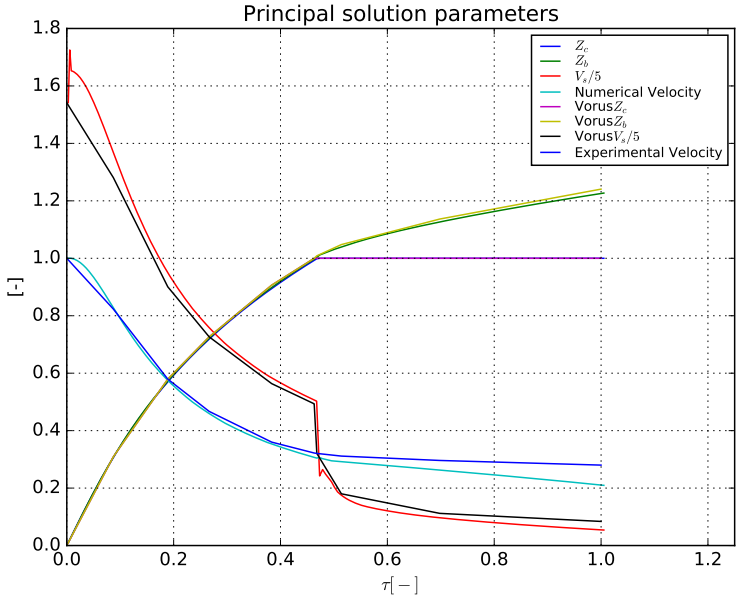

Figure 5.10: Principal Solution Parameters with old γ definition: $C_m = 0.5$

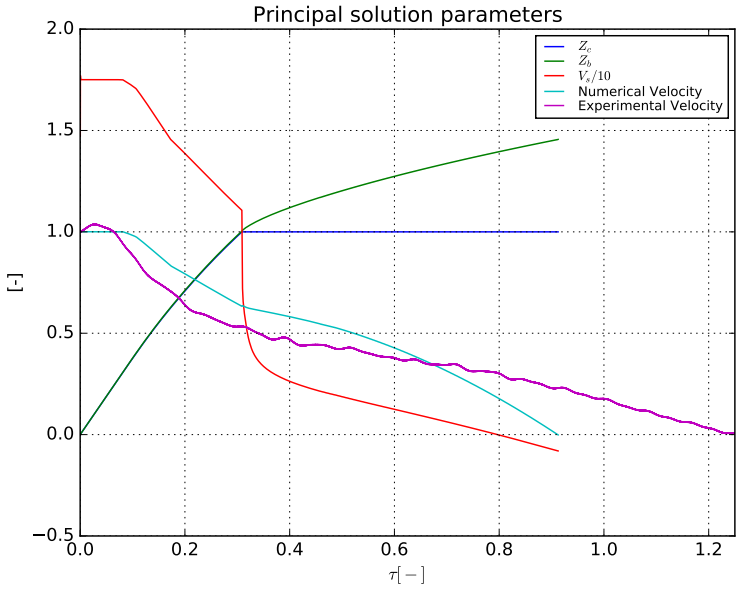

Figure 5.11: Principal Solution parameter: 0.152 meter drop height

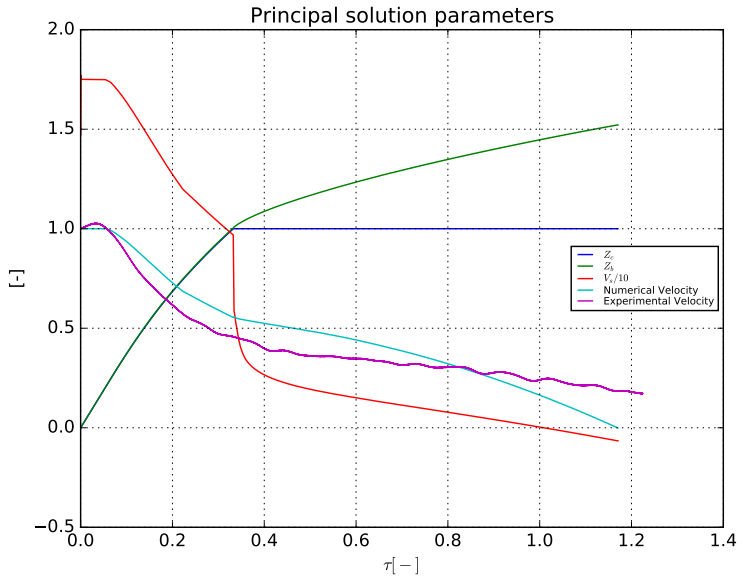

Figure 5.12: Principal Solution parameter: 0.305 meter drop height

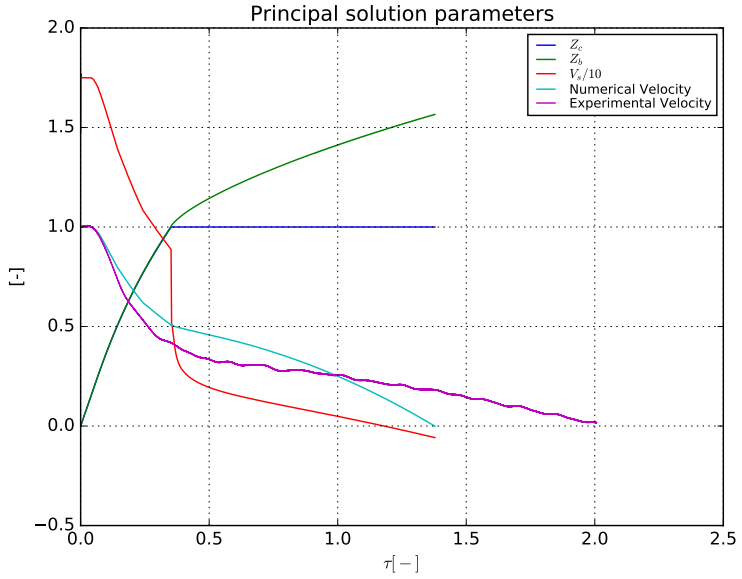

Figure 5.13: Principal Solution parameter: 0.457 meter drop height

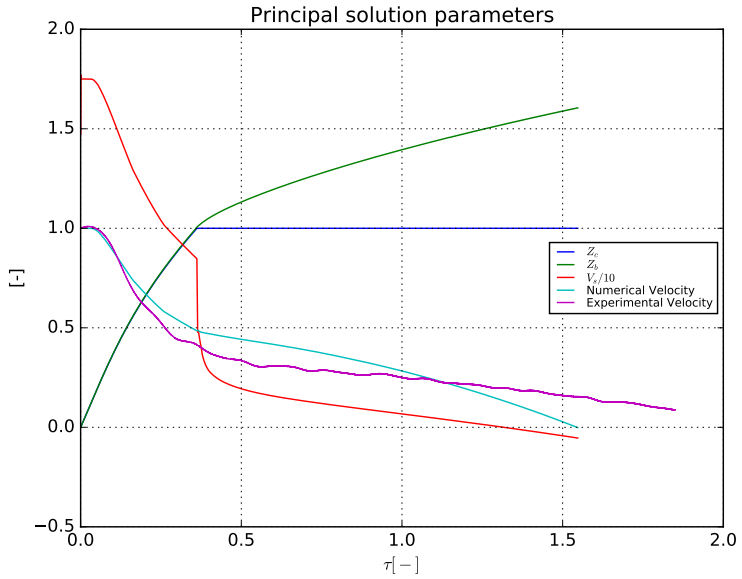

Figure 5.14: Principal Solution parameter: 0.609 meter drop height

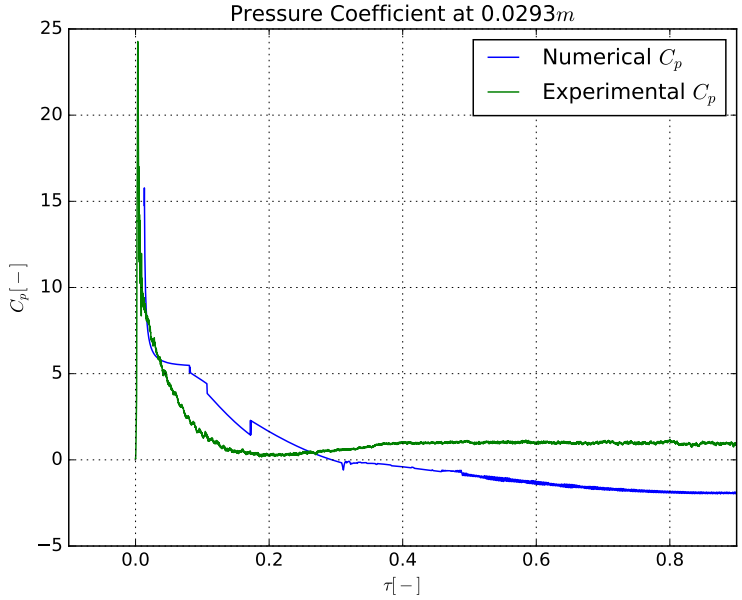

Figure 5.15: C_p at $0.0293m$ from keel: 0.152 meter drop height

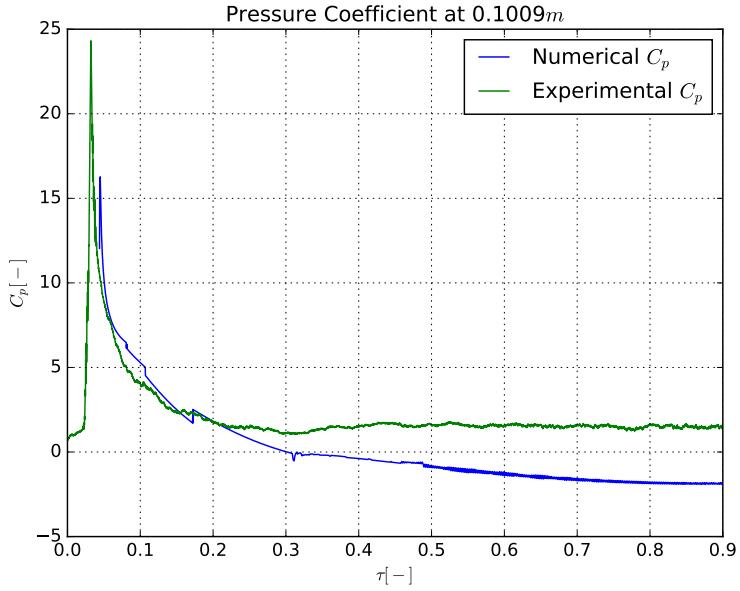

Figure 5.16: C_p at $0.1009m$ from keel: 0.152 meter drop height

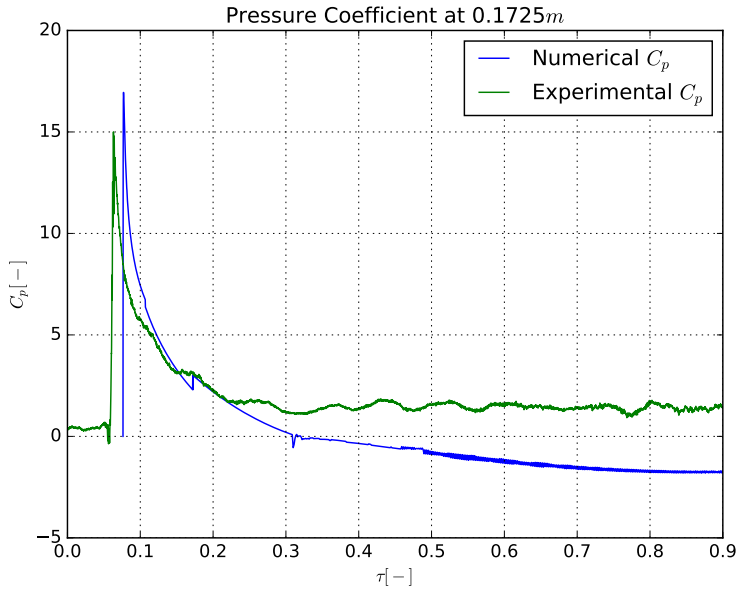

Figure 5.17: C_p at $0.1725m$ from keel: 0.152 meter drop height

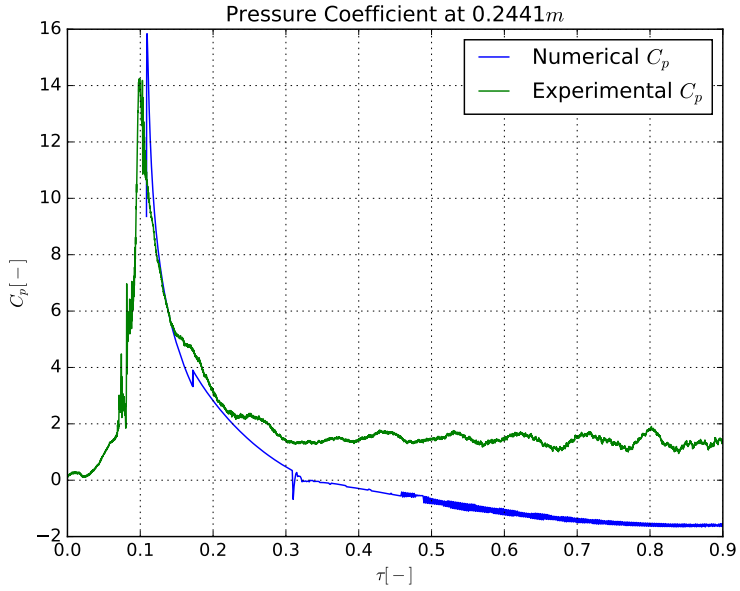

Figure 5.18: C_p at $0.2441m$ from keel: 0.152 meter drop height

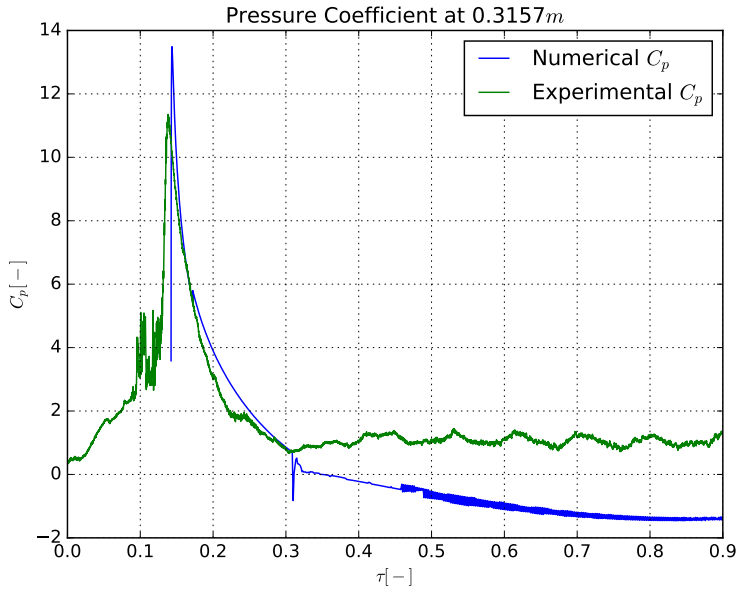

Figure 5.19: C_p at $0.3157m$ from keel: 0.152 meter drop height

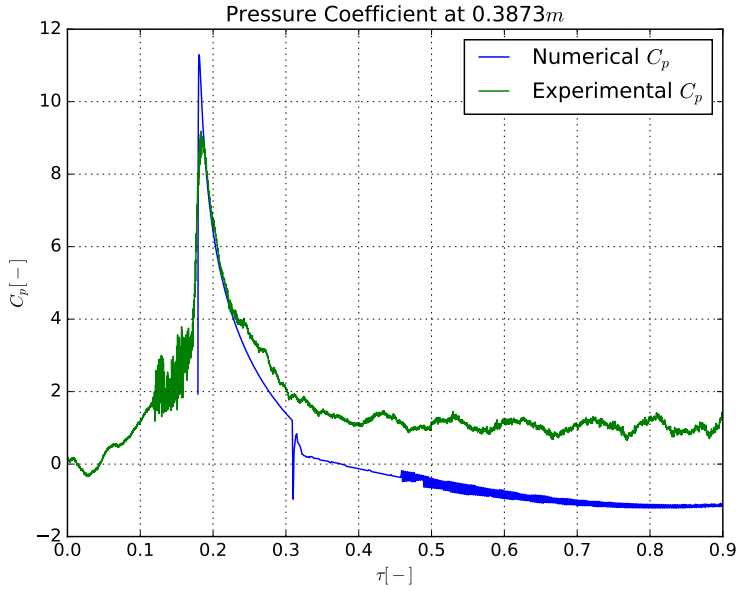

Figure 5.20: C_p at $0.3873m$ from keel: 0.152 meter drop height

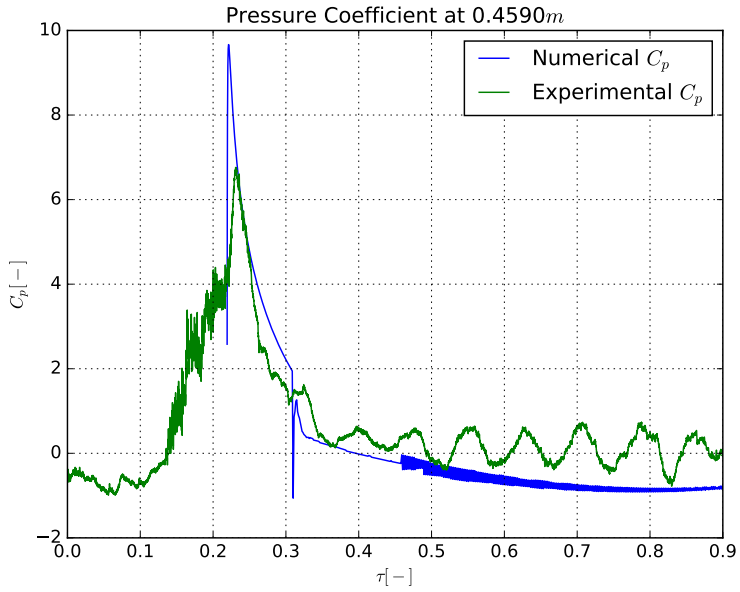

Figure 5.21: C_p at $0.4590m$ from keel: 0.152 meter drop height

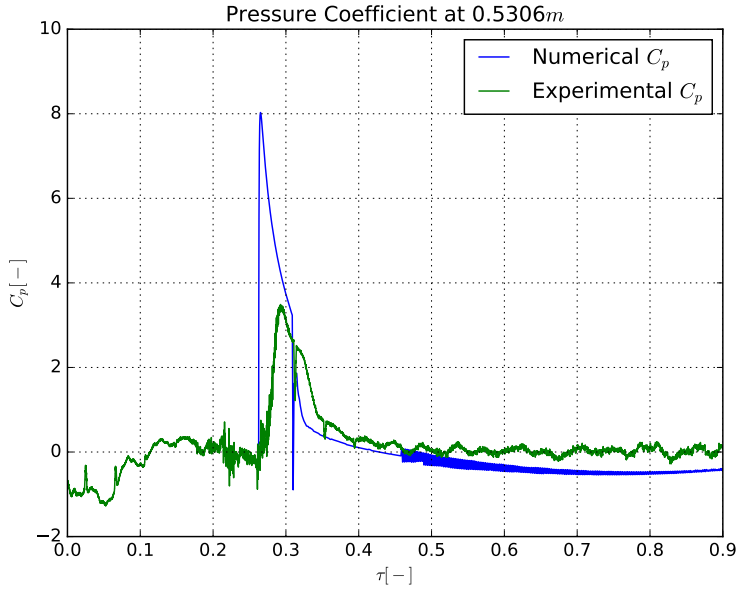

Figure 5.22: C_p at $0.5306m$ from keel: 0.152 meter drop height

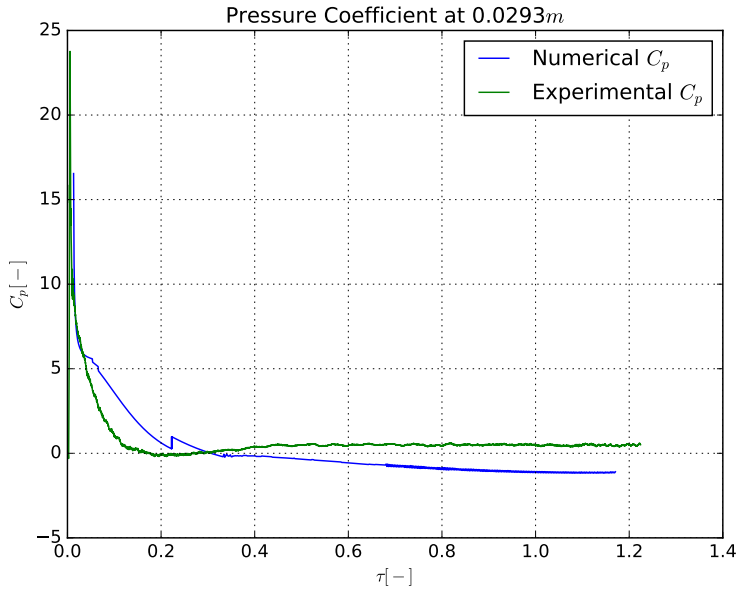

Figure 5.23: C_p at $0.0293m$ from keel: 0.305 meter drop height

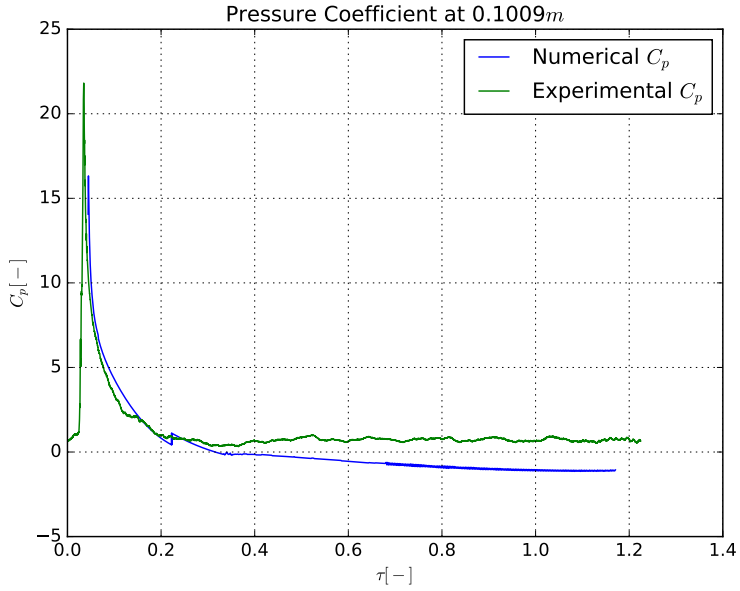

Figure 5.24: C_p at $0.1009m$ from keel: 0.305 meter drop height

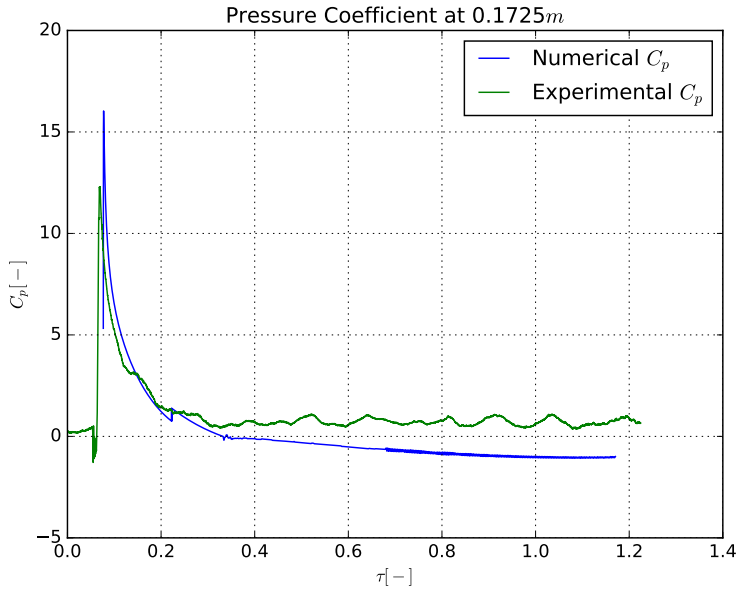

Figure 5.25: C_p at $0.1725m$ from keel: 0.305 meter drop height

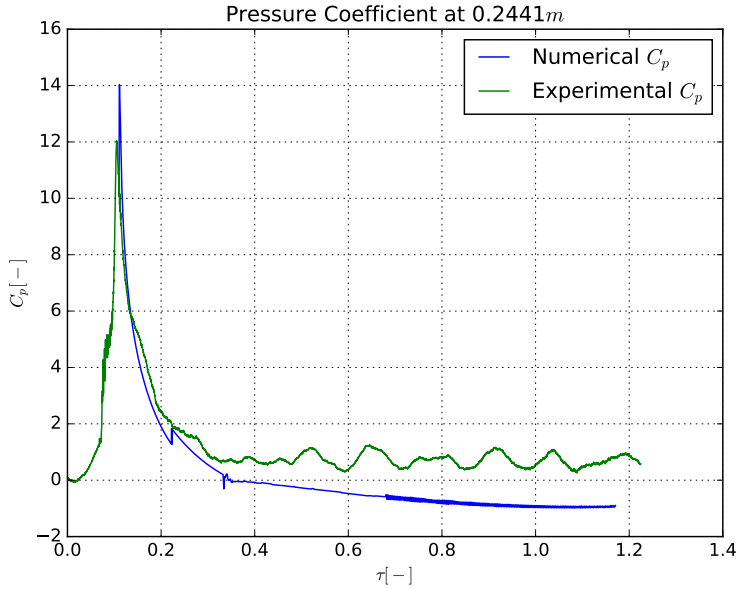

Figure 5.26: C_p at $0.2441m$ from keel: 0.305 meter drop height

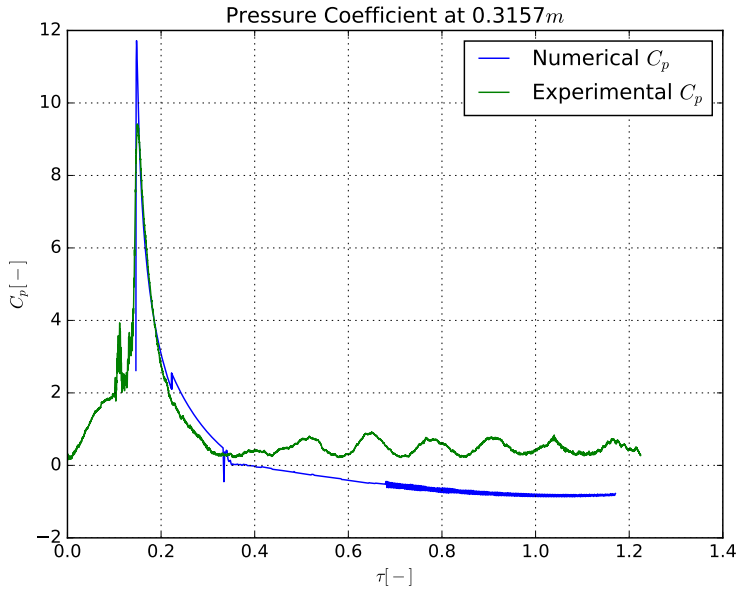

Figure 5.27: C_p at $0.3157m$ from keel: 0.305 meter drop height

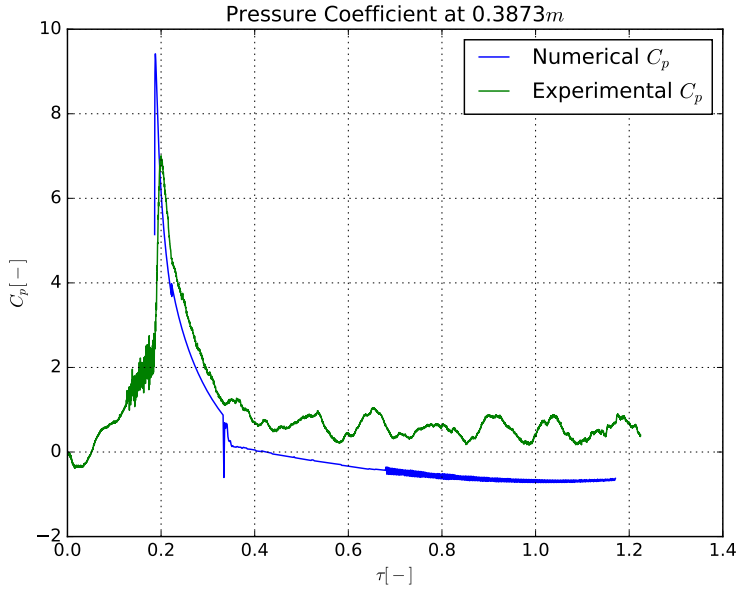

Figure 5.28: C_p at $0.3873m$ from keel: 0.305 meter drop height

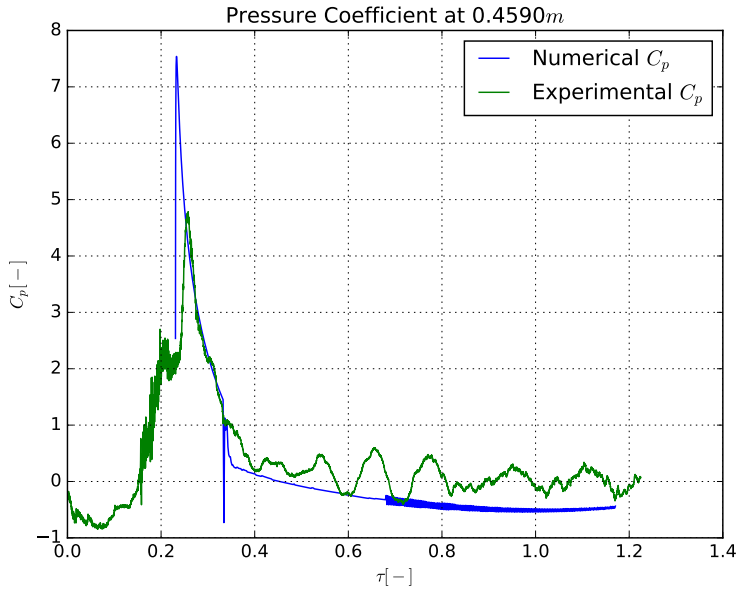

Figure 5.29: C_p at $0.4590m$ from keel: 0.305 meter drop height

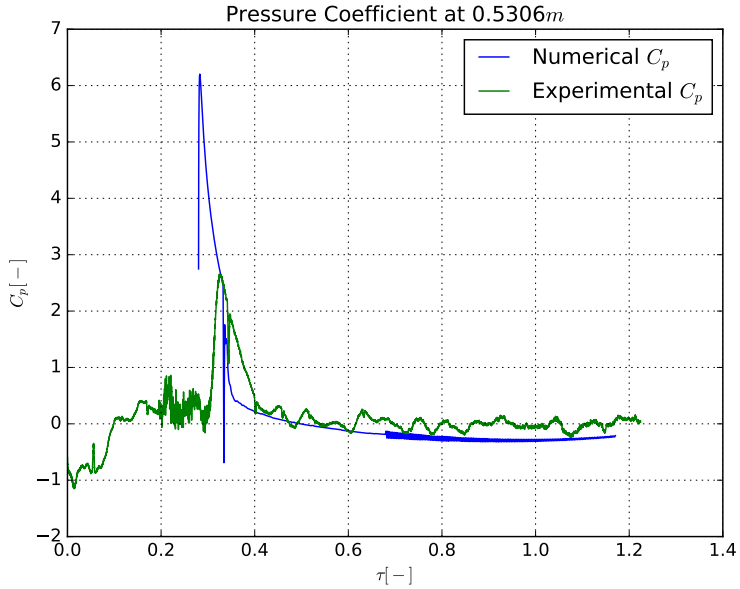

Figure 5.30: C_p at $0.5306m$ from keel: 0.305 meter drop height

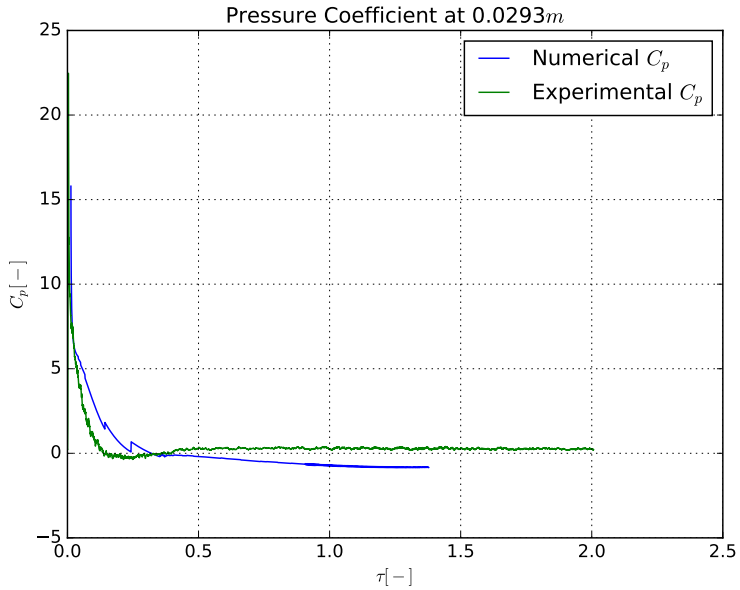

Figure 5.31: C_p at $0.0293m$ from keel: 0.457 meter drop height

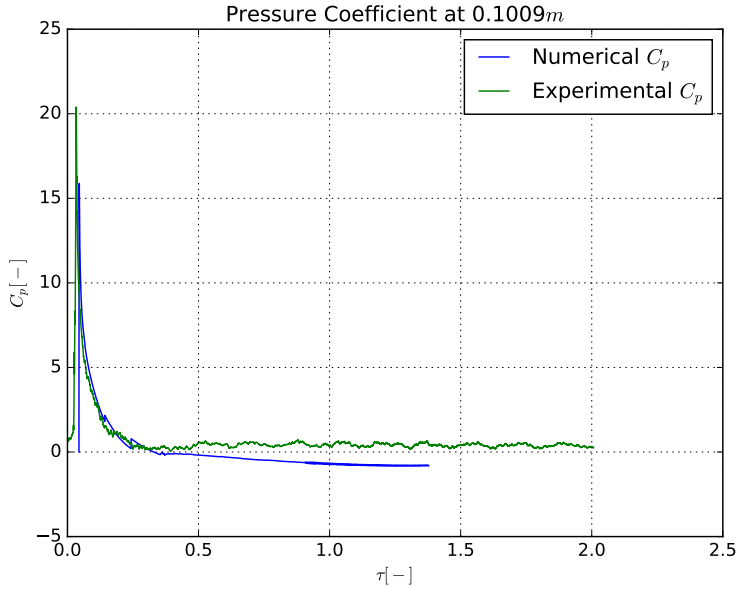

Figure 5.32: C_p at $0.1009m$ from keel: 0.457 meter drop height

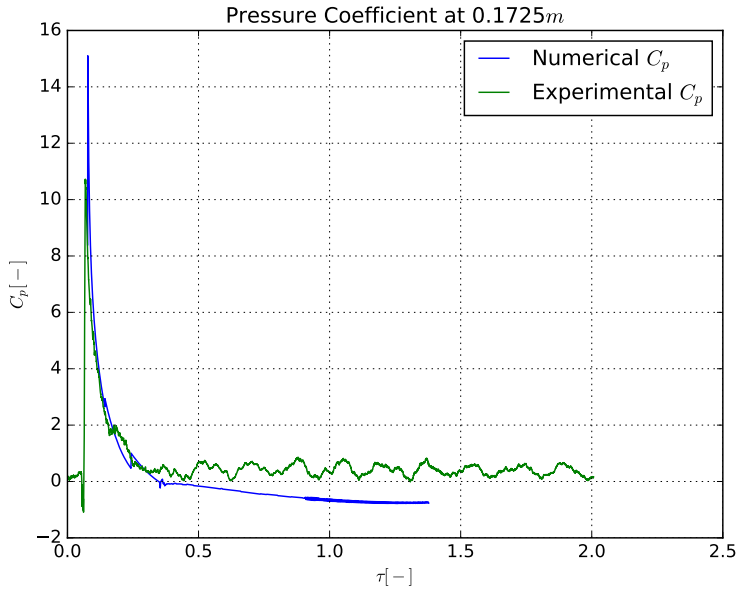

Figure 5.33: C_p at $0.1725m$ from keel: 0.457 meter drop height

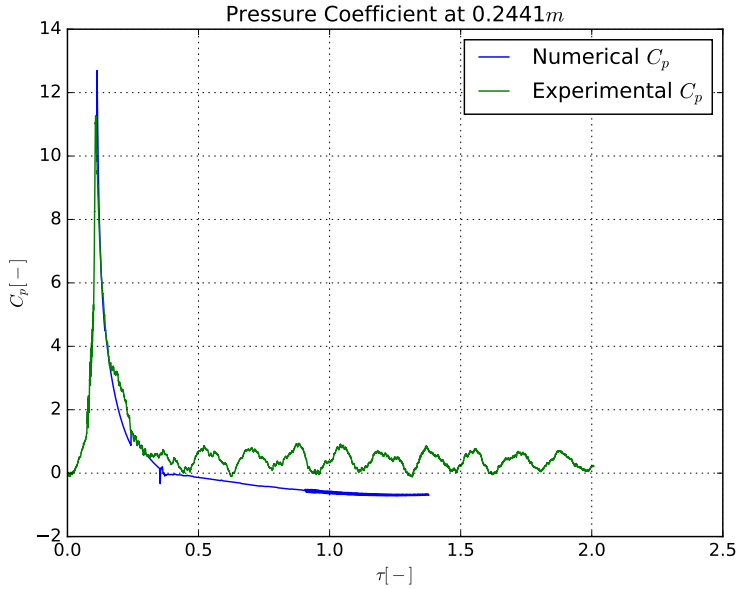

Figure 5.34: C_p at $0.2441m$ from keel: 0.457 meter drop height

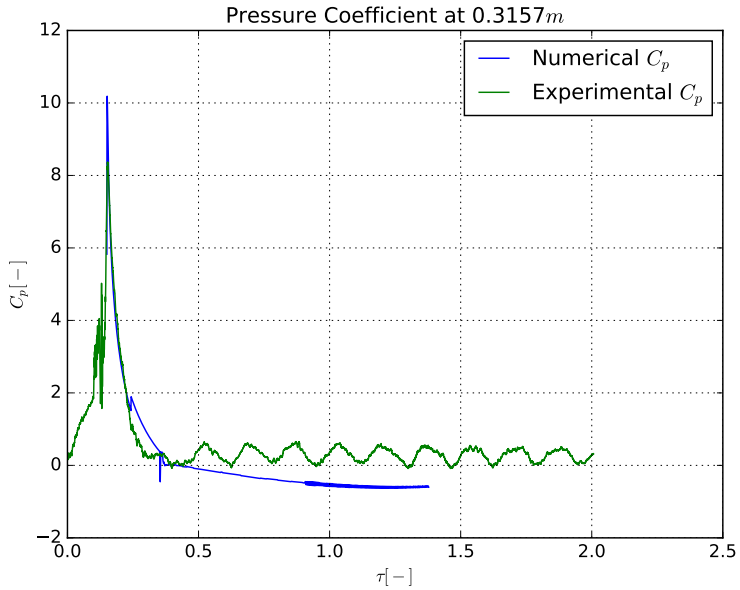

Figure 5.35: C_p at $0.3157m$ from keel: 0.457 meter drop height

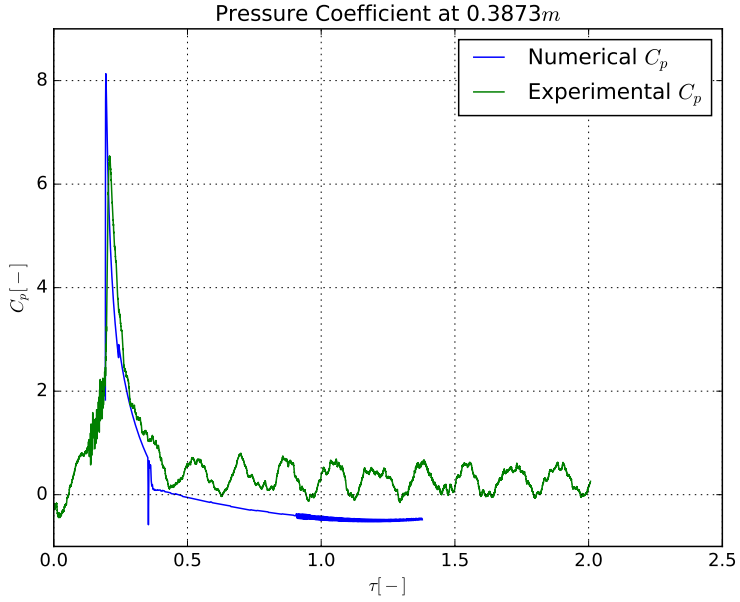

Figure 5.36: C_p at $0.3873m$ from keel: 0.457 meter drop height

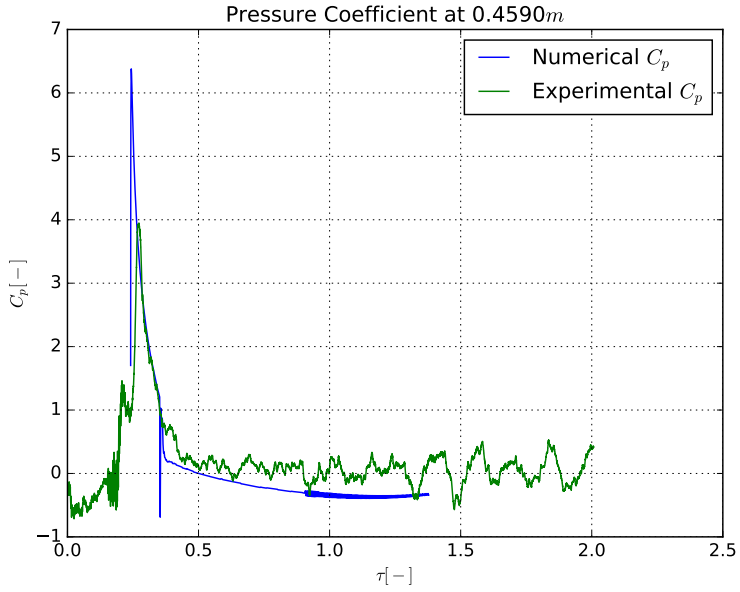

Figure 5.37: C_p at $0.4590m$ from keel: 0.457 meter drop height

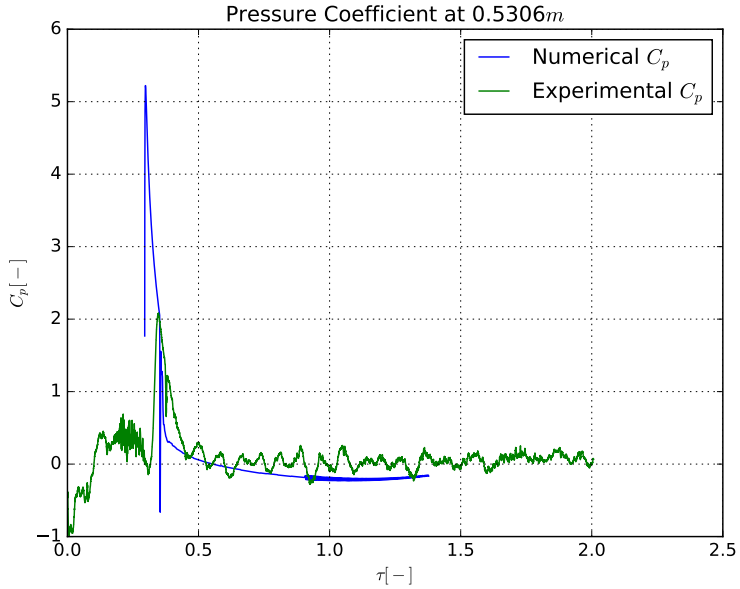

Figure 5.38: C_p at $0.5306m$ from keel: 0.457 meter drop height

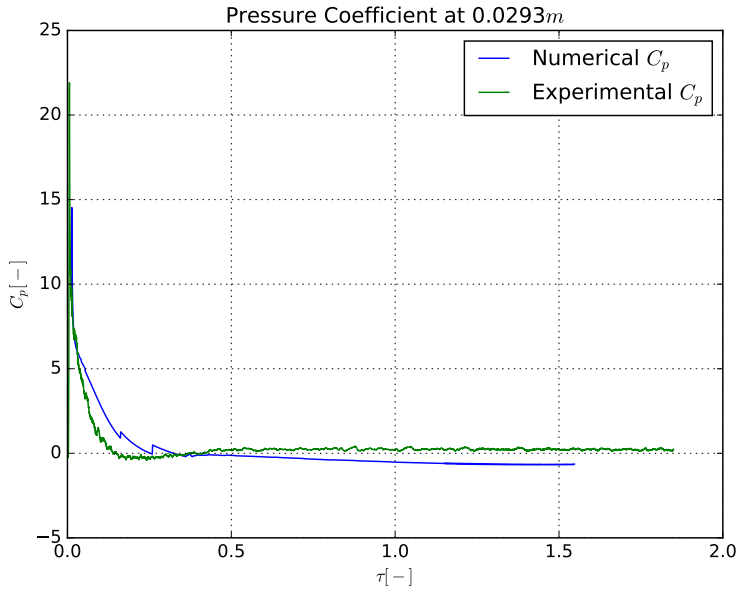

Figure 5.39: C_p at $0.0293m$ from keel: 0.609 meter drop height

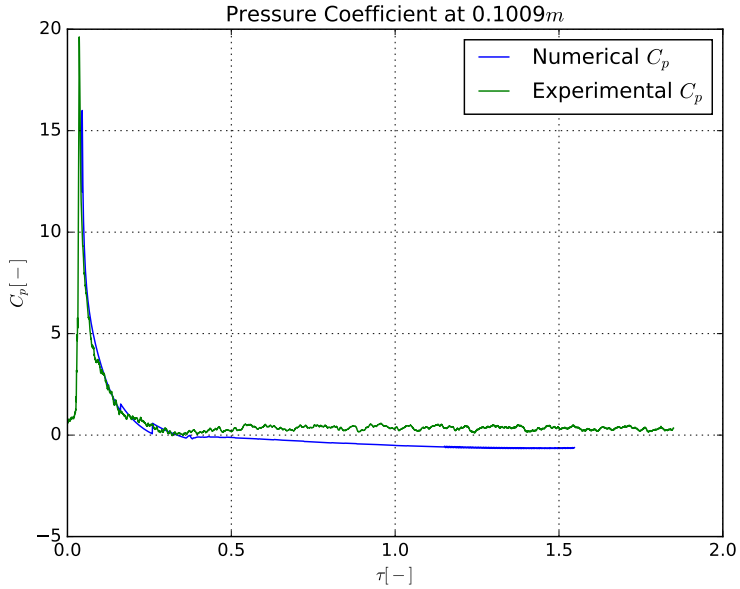

Figure 5.40: C_p at $0.1009m$ from keel: 0.609 meter drop height

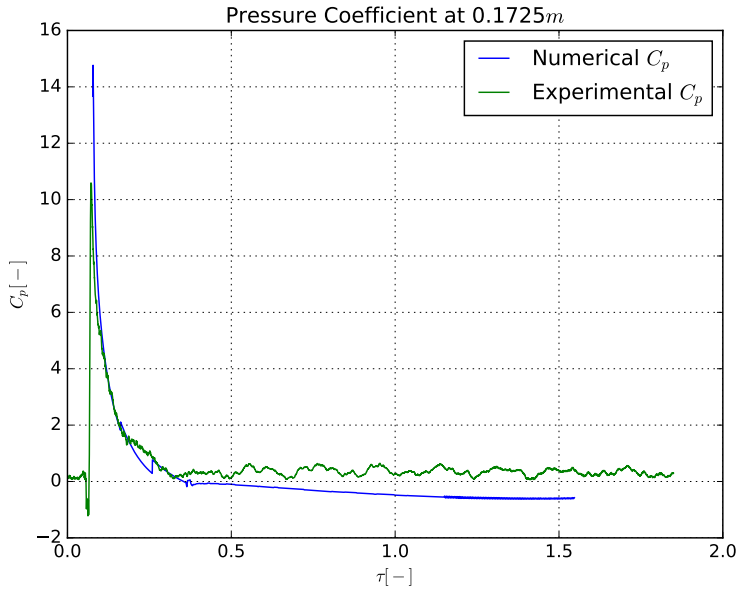

Figure 5.41: C_p at $0.1725m$ from keel: 0.609 meter drop height

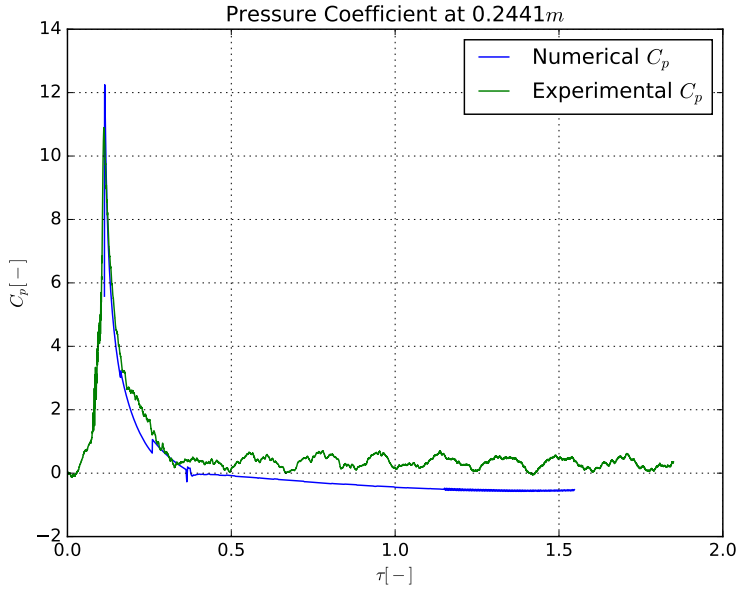

Figure 5.42: C_p at $0.2441m$ from keel: 0.609 meter drop height

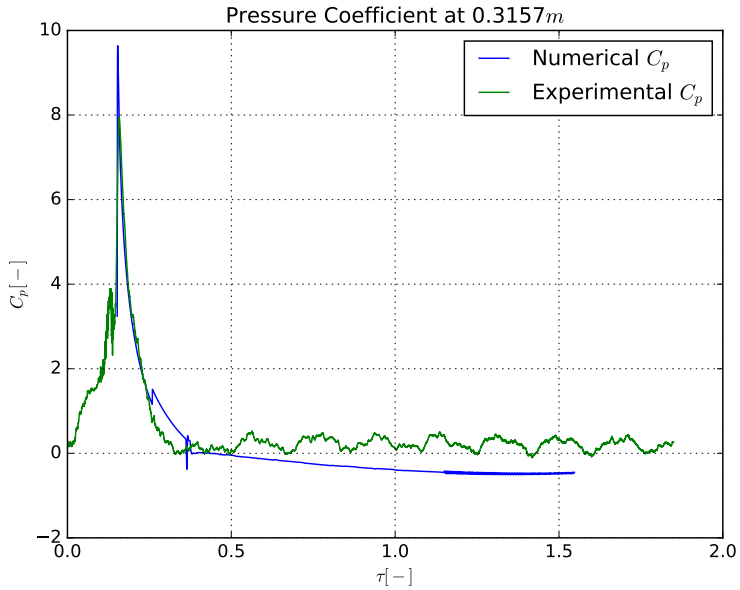

Figure 5.43: C_p at $0.3157m$ from keel: 0.609 meter drop height

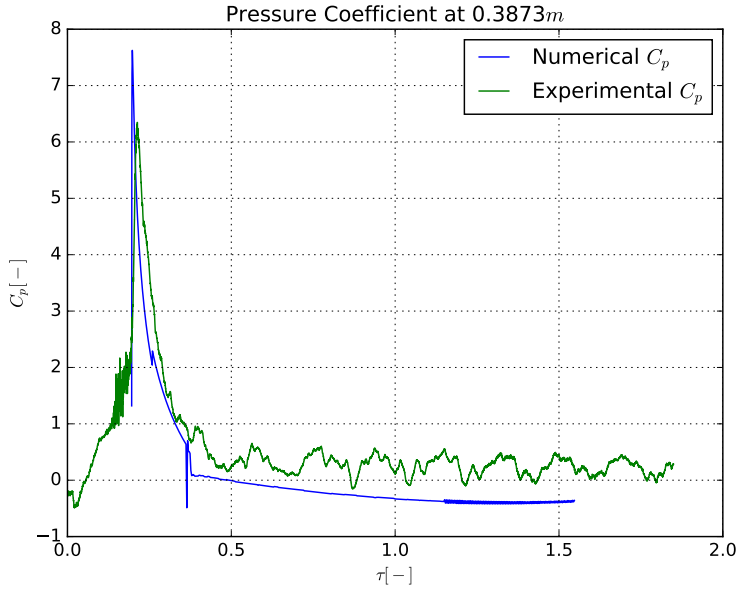

Figure 5.44: C_p at 0.3873m from keel: 0.609 meter drop height

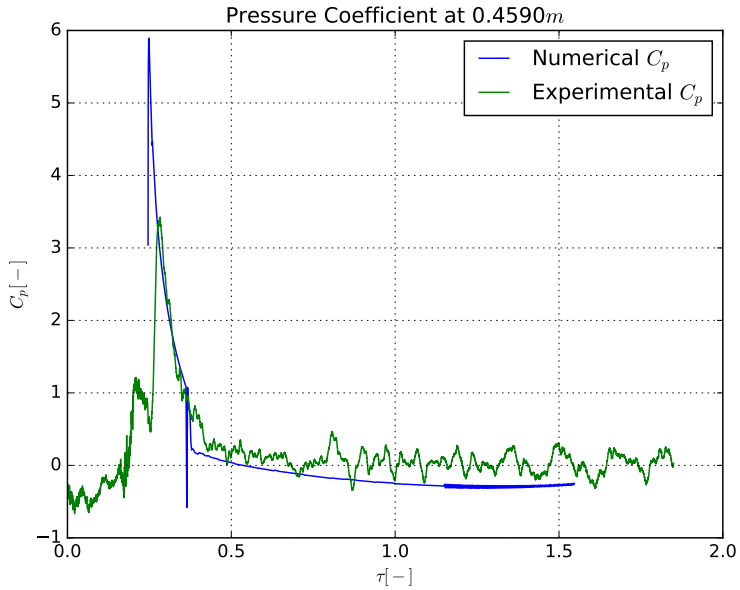

Figure 5.45: C_p at 0.4590m from keel: 0.609 meter drop height

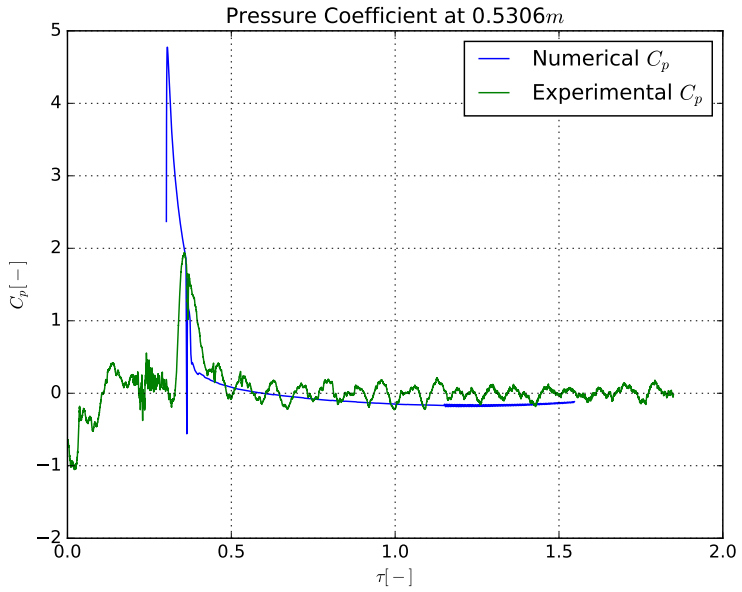

Figure 5.46: C_p at 0.5306m from keel: 0.609 meter drop height

Chapter 6

Conclusion

The numerical development of this computer code is an extension to theory developed by Vorus (1996) to increase the predictive capabilities for analysis of planing surface crafts in association to the recent developments by Savander et al. (2002). This numerical and experimental study in comparison with research conducted previously such in Dobrovol'skaya (1969), Zhao and Faltinsen (1993), Vorus (1996), and Savander et al. (2002) validates the working of code and forms a basis for further development of an economical and user friendly computer code that can be used in industry for analysis and design of high-speed planing crafts. As discussed in Chapter 5 the hydrodynamic pressures created by jet rise do not increase with increasing impact velocities as also stated by Eastridge (2017). However, once the forces acting on the bottom plating are predicted as shown in Chapter 3, the deflection in bottom plating can be easily predicted and data can be used in the study of hydroelasticity of the bottom shell plating.

This study forms a basic understanding of the non-linear equations to formulate boundary-value problem in the time domain. The code developed gives a procedure and sequential steps to solve these equations iteratively. The results obtained as shown in Chapter 3 agree with the experimental values or at least follow the basic trend seen. As seen the velocity of the cylinder is predicted within the range of 4% to 20% of difference. The difference reduces as the impact velocity. The peak pressures predicted are within the range of -32.8% to 62.1% difference. The difference are high but the absolute difference is small. It is also seen from Figures 5.11 to 5.46 that code works better for CUW phase because as emphasized in chapter 3 there is hard discontinuity in geometry during CW phase, which is better tackled

by analytical solution than numerical solution. During experimentation, three dimensional effects of the impact was also observed visually which is not considered in this study yet. More work needs to be done on iterative schemes used in the code with refinement in allocation techniques to handle higher discretization of contour. The subroutines to handle variable deadrise angle along $z - axis$. Further for analysis of steady planing via slender body theory, as demonstrated by Tulin (1957) for prismatic hull, Vorus (1996) provides an extension for nonzero dead-rise angle. The sections of boat are considered to pass through fixed frame of reference are considered to be as impacting two-dimensional contours with impact velocity as $U \tan \alpha(x)$, U is the forward steady boat speed and $\alpha(x)$ is trim angle along $x - axis$ longitudinally, hence the coordinates can be transformed from impact to planing for application of strip theory as seen in Savander et al. (2002). Using this relation between time-domain impact and steady planing flow, would require incorporation of time varying contour geometry in the theory as well.

References

Cointe, R. (1991). "Free surface flow close to surface piercing body". In: *J. Fluid Mech. 36 805.*

Dobrovol'skaya, Z. N. (1969). "On some problems of similarity flow of fluid with a free surface". In: *Mathematical Approach in Hydrodynamics 319-334.*

Eastridge, Jonathan R. (2017). "An Experimental Study in the Hydroelastic Response of an Aluminum Wedge in Drop Tests". Theses and Dissertations. University of New Orleans. URL: `https://scholarworks.uno.edu/td/2317`.

I.S.Gradshteyn and I.M. Ryzhik (1965). "Table of Integrals,Series and Products". In: *Academinc Press, New York.*

Judge, C. et al. (2004). "Initial water impact of a wedge at vertical and oblique angles". In: *Journal of Engineering Mathematics, Vol 48, pp 279-303.*

Karman, T. von (1929). "Impact of seaplane floats during landing". In: *NACA TN 321.*

Savander, Brant R. et al. (2002). "Steady Hydrodynamic Analysis of Planing Surfaces". In: *Journal Of Ship Research.*

Tulin, M. (1957). "Theory of slender planing surfaces at high speeds". In: *Schiffstechnik.*

Vorus, William S. (1996). "A Flat Cylinder Theory for Vessel Impact and Steady Planing Resistance". In: *Journal Of Ship Research.*

— (2017). *Hydrodynamics of Planing Monohull Watercraft.* Philadelphia: Springer Briefs In Applied Sciences and Technology.

Wagner, H. (Aug. 1932). "Uber stoss-und gleitvorgangean der oberflanche von flussigkeiten". In: *Zeitschrift für Angewandte Mathematik und Mechanik* 12.

Zhao, R. and O. Faltinsen (1993). "Water entry of two-dimensional bodies". In: *Journal Of Fluid Mechanics.*

Vita

The author was born in city of Lucknow in India. He passed his early school in capital New Delhi and later on obtained his Bachelor's degree in Marine Engineering from Birla Institute Of Technology and Sciences, India in 2014. After graduation he worked as Marine Engineer Officer on various merchant ships. In Fall, 2016 he came to University of New Orleans to pursue master's in Naval Architecture and Marine Engineering. He is now pursuing Ph.D. at University of New Orleans in Engineering and Applied Science.